A Plant-Specific N-terminal Extension Reveals Evolutionary Functional Divergence within Translocator Proteins

Pawel Jurkiewicz, Lucile Senicourt, Haitham Ayeb, Olivier Lequin, Jean-Jacques Lacapere, Henri Batoko

iScience

CellPress

Article

A Plant-Specific N-terminal Extension Reveals Evolutionary Functional Divergence within Translocator Proteins

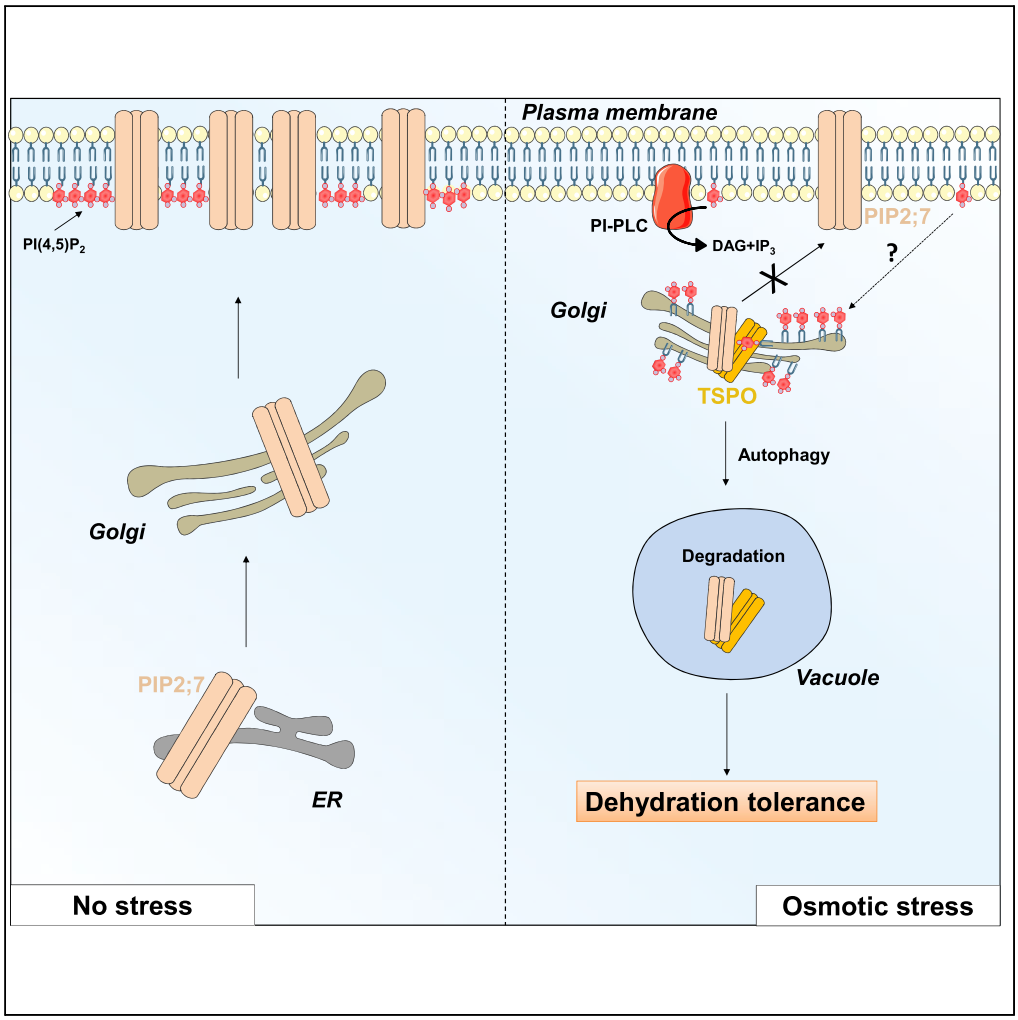

Pawel Jurkiewicz, Lucile Senicourt, Haitham Ayeb, Olivier Lequin, Jean-Jacques Lacapere, Henri Batoko

henri.batoko@uclouvain.be

HIGHLIGHTS

Plant TSPOs possess a specific and structurally conserved polybasic N-terminal extension

Plant TSPOs bind PI(4,5)P_2 *in vitro* and at the Golgi membrane *in vivo*

The polybasic N-terminal extension is required for PI(4,5)P_2 binding

Plant TSPO depletes the plasma membrane of both an aquaporin and a PI(4,5)P_2

Jurkiewicz et al., iScience *23*, 100889
March 27, 2020
https://doi.org/10.1016/j.isci.2020.100889

iScience

CellPress

Article

A Plant-Specific N-terminal Extension Reveals Evolutionary Functional Divergence within Translocator Proteins

Pawel Jurkiewicz,[1,4] Lucile Senicourt,[2,3] Haitham Ayeb,[1] Olivier Lequin,[2] Jean-Jacques Lacapere,[2] and Henri Batoko[1,5,*]

SUMMARY

Conserved translocator proteins (TSPOs) mediate cell stress responses possibly in a cell-type-specific manner. This work reports on the molecular function of plant TSPO and their possible evolutionary divergence. *Arabidopsis thaliana* TSPO (AtTSPO) is stress induced and has a conserved polybasic, plant-specific N-terminal extension. AtTSPO reduces water loss by depleting aquaporin PIP2;7 in the plasma membrane. Herein, AtTSPO was found to bind phosphoinositides *in vitro*, but only full-length AtTSPO or chimeric mouse TSPO with an AtTSPO N-terminus bound $PI(4,5)P_2$ *in vitro* and modified PIP2;7 levels *in vivo*. Expression of AtTSPO but not its N-terminally truncated variant enhanced phospholipase C activity and depleted $PI(4,5)P_2$ from the plasma membrane and its enrichment in Golgi membranes. Deletion or point mutations within the AtTSPO N-terminus affected $PI(4,5)P_2$ binding and almost prevented AtTSPO-PIP2;7 interaction *in vivo*. The findings imply functional divergence of plant TSPOs from bacterial and animal counterparts via evolutionary acquisition of the phospholipid-interacting N-terminus.

INTRODUCTION

Translocator proteins (TSPOs) are polytopic membrane proteins present in organisms from prokaryotes to humans (Kreps et al., 2002; Seki et al., 2002; Zimmermann et al., 2004; Papadopoulos et al., 2006; Guillaumot et al., 2009; Fan et al., 2012; Guo et al., 2015; Li et al., 2015). TSPOs share an evolutionarily conserved structure consisting of five α-helical transmembrane segments forming a tryptophan-rich sensory protein/mitochondrial benzodiazepine receptor (TspO/MBR) domain (Fan et al., 2012; Jaremko et al., 2014; Guo et al., 2015; Li et al., 2015). TSPOs are attracting clinical and pre-clinical research attention due to links to human diseases such as metastatic cancer, central nervous system (CNS) ailments including Alzheimer and Parkinson, and neuroinflammations (Papadopoulos et al., 2006; Rupprecht et al., 2010; Gatliff et al., 2017). Natural and synthetic TSPO ligands are widely used as diagnostic tools and treatments for the aforementioned conditions despite the molecular functions remaining unknown (Rupprecht et al., 2010; Morin et al., 2016). Although TSPOs have been extensively studied since their discovery in the 1970s (Braestrup and Squires, 1977), varying findings across species and experimental models have failed to clarify evolutionarily conserved molecular functions. Functional studies of bacterial, mammalian, and plant TSPOs indicate roles in sensing and stress responses (Yeliseev and Kaplan, 1999; Davey and de Bruijn, 2000; Guillaumot et al., 2009; Jaremko et al., 2014; Guo et al., 2015; Li et al., 2015).

In bacteria, TSPOs are involved in responses to nutrient deficiency, stress-related and light-dependent processes such as the synthesis of photosynthetic pigments, and oxygen-dependent respiration (Yeliseev and Kaplan, 1999; Davey and de Bruijn, 2000). Interestingly, a phylogenetically distant rat TSPO rescued the phenotype of a knockout mutant of the photosynthetic bacteria *Rhodobacter sphaeroides*, indicating functional as well as structural conservation (Yeliseev et al., 1997). In eukaryotes, TSPOs are localized in different intracellular membrane compartments, and deletion of mitochondria-localized *Schizosaccharomyces pombe* TSPO (SpTSPO) enhanced sensitivity to mineral toxicity and to the drug rapamycin (Doi et al., 2015). Rapamycin and its derivatives are therapeutically attractive immunosuppressants and antitumor agents (Augustine et al., 2007) that function by inhibiting the mechanistic target of rapamycin (mTOR), a key kinase regulating starvation-induced autophagy in eukaryotic cells (Weisman and Choder, 2001;Thoreen et al., 2009; Sancak et al., 2010;Nakashima et al., 2010). In addition, rapamycin may serve as a calorie restriction mimetic to extend lifespan (Takahara and Maeda, 2013). Overexpression of SpTSPO

[1]Louvain Institute of Biomolecular Science and Technology (LIBST), University of Louvain (UCLouvain), Croix du Sud 4-5, L7.07.14, 1348 Louvain-la-Neuve, Belgium

[2]Sorbonne Université, École Normale Supérieure, PSL University, CNRS, Laboratoire des Biomolécules, 4 Place Jussieu, 75005 Paris, France

[3]Present address: Structure et Fonction de Protéines hautement Flexibles, Center de Biochimie Structurale, CNRS UMR 5048 - UM 1 - INSERM UMR 1054, 29 rue de Navacelles, 34090 Montpellier Cedex, France

[4]Present address: Strand Associates Consulting, Italiëlei 88, 2000 Antwerpen, Belgium

[5]Lead Contact

*Correspondence: henri.batoko@uclouvain.be

https://doi.org/10.1016/j.isci.2020.100889

increases cell viability at stationary phase, and deletion of SpTSPO decreases cell population growth on glucose (Doi et al., 2015). Interestingly, inhibition or knockdown of Drosophila TSPO (dTSPO) inhibits wing disk apoptosis in response to γ-irradiation or H_2O_2 exposure, extends fly lifespan, and reduces neurodegeneration (Lin et al., 2014). In multiple cross-species cell types, TSPO overexpression stimulates an oxidative cellular environment, which is reversed upon knockdown (Vanhee et al., 2011a; Doi et al., 2015; Batoko et al., 2015; Gatliff et al., 2017). TSPO expression is transiently increased during inflammation of the CNS, facilitating imaging using functionalized TSPO-specific ligands (Braestrup and Squires, 1977; Rupprecht et al., 2010). For example, animal TSPO is abundantly expressed in glial cells recruited and activated during neuroinflammation, where it may modulate redox homeostasis (Hong et al., 2006; Lavisse et al., 2012; Banati et al., 2014; Bae et al., 2014; Liu et al., 2015). Involvement of TSPO in reactive oxygen species (ROS) signaling may be linked to porphyrin binding (Batoko et al., 2015; Guo et al., 2015; Margineedas-Freixa et al., 2016; Ozaki et al., 2010; Vanhee et al., 2011; Verma et al., 1987; Guilarte et al., 2016), because porphyrins are the main endogenous ligands of TSPO in all cell types, and free protoporphyrins are powerful light-dependent ROS generators.

Although TSPO ligands are applied in clinical imaging and therapeutics, TSPO functions remain poorly understood (Li et al., 2016). Mammalian mitochondrial TSPO and the mitochondrial outer membrane partner voltage-dependent anion channel (VDAC1) contribute to establishing a molecular platform for tuning autophagy-mediated removal of ROS-damaged mitochondria (Gatliff et al., 2014). *Arabidopsis thaliana* TSPO (AtTSPO) is transiently induced by abiotic (osmotic) stress and the stress phytohormone abscisic acid (ABA) (Kreps et al., 2002; Seki et al., 2002; Guillaumot et al., 2009; Vanhee et al., 2011a). The time-limited presence of AtTSPO in plant cells may contribute to osmotic stress responses. Indeed, the mostly Golgi-localized AtTSPO physically interacts with the highly expressed plasma membrane (PM) aquaporin PIP2;7 in both Golgi and ER membranes (Hachez et al., 2014). Under osmotic stress, AtTSPO interacts with PIP2;7 *en route* to the PM, thereby contributing to reducing water loss (Hachez et al., 2014). The resulting protein complex is subsequently targeted to the vacuole via the autophagic pathway. Plant TSPO may act as a selective autophagy receptor targeting haem and aquaporin to the vacuole for degradation (Vanhee et al., 2011b; Hachez et al., 2014). The underlying molecular mechanisms of these interactions are not clear yet, but TSPO involvement in stress homeostasis could be a conserved ancestral function, albeit with species dependent mechanistic variation (Batoko et al., 2015; Li et al., 2016). TSPOs may be ancient bacterial receptor/stress sensors that have evolved additional interactions, partners, and roles in eukaryotes (Li et al., 2016).

Terrestrial plants lose water primarily through pores in their aerial parts known as stomata. Turgor and nonturgidity of stomatal guard cells respectively determine pore opening and closing (Mishra et al., 2006). ABA-dependent regulation of stomata involves changes in ROS, calcium, the cytoskeleton, and signaling phosphoinositides (Schroeder et al., 2001; Hetherington and Brownlee, 2004; Lee et al., 2007; Cutler et al., 2010). Dynamic pools of phosphoinositides (PIs), a family of phospholipids located on the cytoplasmic leaflet of cellular membranes, mediate key cellular processes such as signal transduction, structural maintenance, motility, endo-exocytosis, autophagy, and regulation of transporter and ion channel function (Hammond et al., 2012; Holthuis and Menon, 2014; Heilmann, 2016). Spatiotemporal remodeling of PI pools within distinct organelles is an intrinsic feature facilitating orchestration of PI-mediated cellular functions (Hammond et al., 2012; Holthuis and Menon, 2014; Heilmann, 2016). Indeed, PIs are regulated by PI-metabolizing enzymes and must be accessible to effectors. Various regulatory proteins including PI effectors bind these negatively charged lipids through specific binding domains or electrostatic interactions (Kooijman et al., 2007; Hammond et al., 2012; Holthuis and Menon, 2014; Munnik and Nielsen, 2011). Subcellular localization of PIs is tightly governed by the concurrent presence of cognate lipid kinases and phosphatases, giving each cellular membrane a unique and dynamic PI signature and contributing to lipid signaling events (Hammond et al., 2012). For instance, the activity of phospholipase Dα1 (PLDα1) and phospholipase C (PLC) generates the messenger lipids phosphatidic acid (PA) and diacylglycerol (DAG), respectively, and both mediate the effects of ABA on stomata opening and closure (Mishra et al., 2006). In particular, PA binds to the negative ABA signaling regulator ABA insensitive 1 (ABI1), a protein phosphatase 2C, to promote stomatal closure, or to the Gα subunit of heterotrimeric G protein to mediate ABA inhibition of stomatal opening (Testerink and Munnik, 2005; Lee et al., 2007).

In the present work, we provide evidence that an evolutionarily conserved plant-specific polybasic N-terminus confers $PI(4,5)P_2$ binding in plant TSPO, and expression of plant TSPO results in $PI(4,5)P_2$

remodeling through its depletion from the PM and enrichment in the Golgi membrane. Physiologically, $PI(4,5)P_2$ binding to plant TSPO is required for physical interaction with PIP2;7 *in vitro* and *in vivo* and subsequent degradation of the protein-lipid complex. Interestingly, addition of the plant-specific polybasic N-terminus to mouse TSPO conferred binding properties to $PI(4,5)P_2$ and, when expressed in plant cells, regulation of PIP2;7 trafficking and abundance in the PM. These findings provide insight into the physiological role of the evolutionary conserved plant-specific polybasic N-terminal extension.

RESULTS

The N-terminal Extension of Arabidopsis TSPO Is Necessary for Protecting Plants against Tissue Dehydration

AtTSPO expression is higher during osmotic stress, but only transiently. We previously showed that AtTSPO physically interacts with defined aquaporin molecules intracellularly, *en route* to the PM, causing a reduction in water transport across the PM during osmotic stress (Hachez et al., 2014). Consistently, we also showed that constitutive expression in plant cells of AtTSPO or the more stable point mutant AtTSPO (H91A) yielded transgenic plants exhibiting reduced water loss compared with wild-type (WT) plants under dehydration. This role in osmotic stress and the underlying molecular mechanism appear to be unique to plant TSPO. Thus, we wondered whether this activity might be associated with the plant-specific N-terminal extension.

To investigate this, we generated transgenic plants overexpressing a truncated version of AtTSPO lacking the first 41 amino acids (p35S::Venus-AtTSPO$^{\Delta N}$) and compared water loss with WT, AtTSPO knockout (KO), and transgenic plants constitutively expressing either AtTSPO (p35S::AtTSPO) or the stable point mutant (p35S::AtTSPO^{H91A}) (Vanhee et al., 2011b). We verified transgene expression in all lines used (Figures 1B and 1D). Under dehydration, KO seedlings had the highest water loss, as expected, whereas p35S::AtTSPO and p35S::AtTSPO^{H91A} plants had the lowest (Figure 1A). Notably, we found no significant difference in water loss between WT and p35S::Venus-AtTSPO$^{\Delta N}$ plants, suggesting deletion of the plant-specific N-terminus abolished the impact of constitutive AtTSPO expression on the regulation of water loss in transgenic plants. Consistent with prior findings (Hachez et al., 2014), tagging the protein at the N-terminus had no effect on regulation of water loss by AtTSPO (also see below).

Water loss is associated with evapotranspiration through stomatal opening, hence we examined stomatal conductance in mature plants also grown on soil. Stomatal conductance measurements on rosette leaves after bolting (Figure 1C) revealed similar trends, indicating that the N-terminal extension is required for regulating water loss mediated by constitutively expressed AtTSPO. Thus, constitutive expression of AtTSPO had a physiological impact on stomatal opening.

The N-terminal Extension of AtTSPO Is Required for Interaction with PIP2;7 *in Planta*

Because AtTSPO-mediated reduction of water loss required the N-terminal extension of AtTSPO and because we previously showed that AtTSPO interacts with PIP2;7 *in vivo* (Hachez et al., 2014), we examined whether the N-terminal extension is required for this interaction *in vivo*. We conducted a bimolecular fluorescence complementation (BiFC) experiment using constructs depicted in Figure 2A. Interaction between the full-length AtTSPO and PIP2;7 containing constructs was readily detectable, but there was no BiFC signal using the truncated AtTSPO construct lacking the first 41 residues at the N-terminus (Figure 2B). As shown previously (Hachez et al., 2014), interaction between AtTSPO and PIP2;7 occurs in Golgi membranes (Figure 2B), and truncated AtTSPO was also localized to Golgi membranes (Figures S1 and S2). Expression of all tested constructs was verified by western blot (Figure 2C), and quantification of the BiFC signal (Figure 2D) indicated that Venus fluorescence detectable with the truncated construct was reduced to that of background levels (see Figure S2 for smaller deletions and Figure S3 for signal quantification methodology). We concluded that truncation of the N-terminus abolished the AtTSPO-PIP2;7 interaction *in vivo*.

Modification of PIP2;7 Abundance at the PM by AtTSPO Requires the Plant-Specific N-Terminal Extension

Because overexpression of AtTSPO drastically reduces the abundance of PIP2;7 at the PM (Hachez et al., 2014), we tested whether the N-terminal extension is required for depletion. We prepared PM-enriched fractions (Figure S4) from Arabidopsis suspension cell lines stably expressing green fluorescent protein

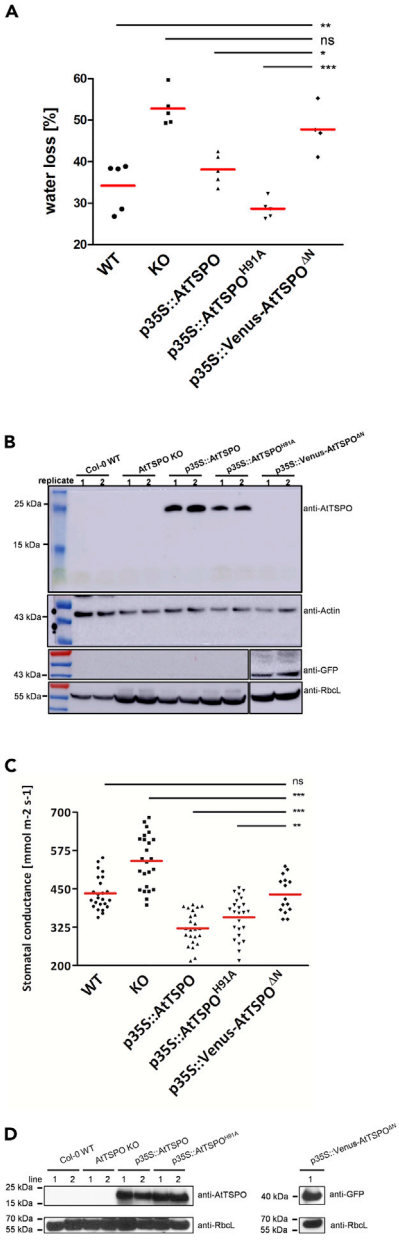

Figure 1. Arabidopsis Plants Expressing N-terminally Truncated AtTSPO Are More Affected by Water Loss than Plants Overexpressing Full-Length AtTSPO

(A) Percentage water loss after 120 min from soil-grown 17-day-old Arabidopsis (whole aerial parts) grown in a phytotron (average temperature 20°C, approx. 65% humidity, 16 h photoperiod, ~120 µmol.m^{-2}.s^{-1}) and dehydrated under light in the same conditions. WT, wild-type; KO, transfer DNA insertional AtTSPO knockout line; p35S::AtTSPO, AtTSPO-overexpressing line; p35S::AtTSPO^{H91A}, transgenic line stably overexpressing AtTSPO harboring point mutation H91A; p35S::Venus-AtTSPO$^{\Delta N}$, line overexpressing Venus-tagged N-terminally truncated AtTSPO. Pooled measurements from five rosettes coming from at least two pots (distributed randomly in the phytotron) are shown, and red horizontal lines define the means for each dataset. Statistical significance was assessed by one-way ANOVA followed by Tukey's tests (*$p < 0.05$; **$p < 0.01$; ***$p < 0.001$; ns, not significant).

(B) Western blot of total protein extracts from rosettes assayed in (A). Per genotype, probed were two replicates (independent pots).

(C) Stomatal conductance of intact leaves from soil-grown mature plants under phytotron conditions. Genotypes are as in (A). Four plants (2–3 rosette leaves per plant) were tested for each line. Individual measurements are shown and red horizontal lines define the means for each dataset. Statistical analysis was conducted as in (A), with **$p < 0.01$.

(D) Western blot of total protein extracts from leaves assayed in stomatal conductance experiments.

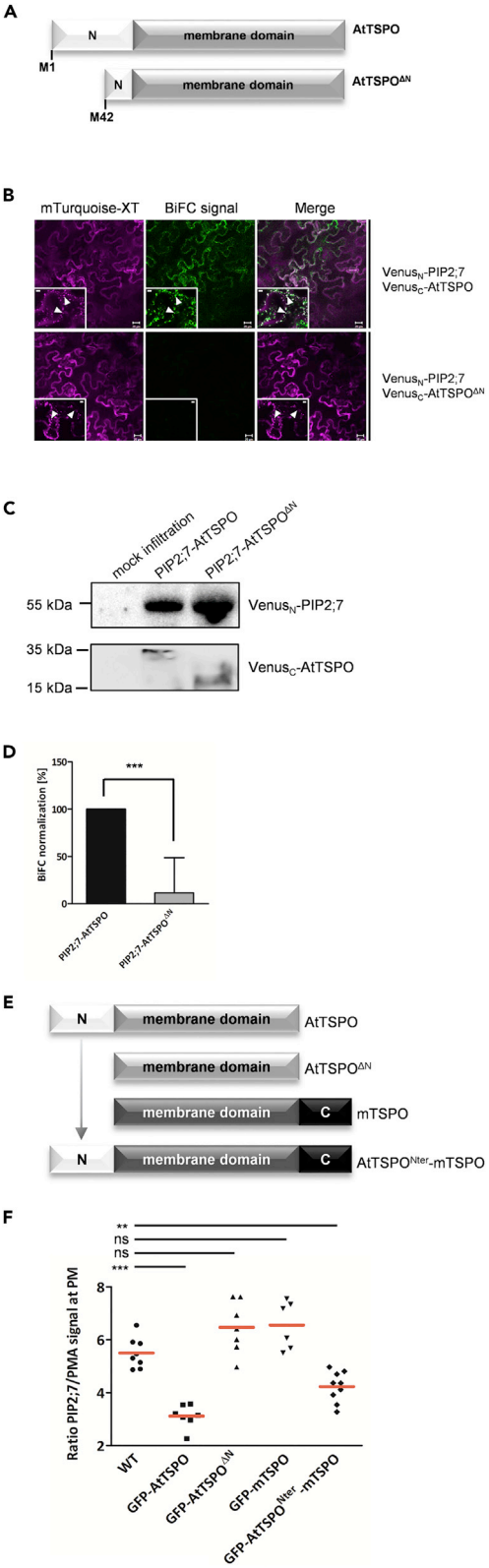

Figure 2. The Plant-specific N-terminal Extension of AtTSPO Is Required for Interaction and Depletion of PIP2;7 *In Vivo*

(A) Schematic representation of AtTSPO genetic constructs prepared for BiFC analysis. Full-length PIP2;7 and AtTSPO served as positive controls. The N-terminally truncated variant starts with methionine at position 42.

(B) Representative confocal images of tobacco epidermal cells transiently coexpressing $Venus_N$-PIP2;7 and $Venus_C$-AtTSPO or $Venus_N$-PIP2;7 and $Venus_C$-AtTSPO$^{\Delta N}$. Xylosyltransferase-mTurquoise fluorescent chimera (magenta) was imaged as a cell transfection control (Golgi marker) and for signal quantification. Low-magnification images qualitatively demonstrate the occurrence or lack of BiFC (green), and insets of high magnification images show Golgi stacks (arrowheads). Bars = 20 μm and 5 μm for low and high magnification, respectively. Experiments were repeated three times.

(C) Western blot of total extracts from infiltrated leaf areas imaged by BiFC. PIP2;7 expression was detected by anti-GFP. Full-length and truncated AtTSPO were detected by anti-FLAG (tag originally cloned between $Venus_C$ and AtTSPO). Non-infiltrated leaf area served as a negative control.

(D) Signal quantification shows a drastic reduction in BiFC, and hence interaction between PIP2;7 and truncated AtTSPO mutant (gray histogram) compared with full-length AtTSPO (black histogram). Bars represent means +/− SD. Statistical significance was assessed by an independent samples t test using Graphpad Prism (***$p < 0.001$).

(E) Schematic representation of genetic constructs stably expressed in Arabidopsis suspension cells. The function of the AtTSPO N-terminus was assessed using the mouse homolog (mTSPO) as a negative control and carrier protein for the plant N-terminus. Each construct was N-terminally tagged with GFP.

(F) PM fractions were extracted from Arabidopsis suspension cells and PIP2;7 was quantified by western blot. PM proton ATPase (PMA) served as a reference protein for signal quantification. Individual measurements (PIP2;7 signal normalized against PMA signal from 6 to 9 replicates from two independent PM preparations) are shown, and the red horizontal lines define the means. Statistical significance was analyzed by t-tests (D) or one-way ANOVA followed by Tukey's tests (**$p < 0.01$; ***$p < 0.001$; ns, not significant) using Graphpad Prism.

(GFP)-tagged full-length AtTSPO and AtTSPO$^{\Delta N}$, and assessed the relative abundance of PIP2;7 by immunoblotting. Consistent with prior findings, the PM fraction from positive control cells expressing full-length AtTSPO exhibited significantly lower amounts of PIP2;7 than did WT cells (Figure 2F). However, no reduction in PIP2;7 levels was seen in AtTSPO$^{\Delta N}$-expressing cells compared with WT cells, suggesting the N-terminal domain of AtTSPO is required for PIP2;7 depletion.

Because the N-terminal extension is unique to plant TSPO, we investigated species specificity by introducing the plant-specific N-terminal extension to the mouse TSPO homolog (mTSPO) by generating a chimeric AtTSPO^{Nter}-mTSPO construct (Figure 2E). As AtTSPO constructs, the chimeric construct also localized within Golgi membranes in plant cells, but unlike the unaltered mTSPO construct that did not decrease PIP2;7 levels, expression of the chimeric construct did diminish PIP2;7 in the PM. However, the efficiency of the reduction (~30%) was lower than that seen with full-length AtTSPO (~60%; Figure 2F), indicating some functional specificity of the N-terminal extension in plants, but also some specificity of the transmembrane domain of AtTSPO vs. mTSPO. We concluded that TSPO-dependent PIP2;7 depletion from the PM requires the plant-specific polybasic N-terminal extension.

AtTSPO Binds Defined Signaling Lipids *In Vitro* via Its Positively Charged N-terminus

The N-terminal extension in higher plant TSPO is rich in arginines and lysines, despite low overall amino acid conservation (Figure 3A). Because positively charged regions may facilitate electrostatic interactions with negatively charged molecules such as anionic lipids (Zheng et al., 2002; Kooijman et al., 2007; Hammond et al., 2012; Holthuis and Menon, 2014; Heilmann, 2016), we hypothesized that AtTSPO-mediated regulation of PIP2;7 levels in the PM may involve interaction between the N-terminal extension of AtTSPO and membrane lipids. We therefore performed lipid overlays using purified full-length AtTSPO and a commercially available membrane spotted with anionic lipids (Figure 3B). Purified AtTSPOs bound all tested PIs except PI(3,4)P_2, as well as phosphatidic acid (PA) and phosphatidylserine (PS; Figure 3B). To confirm the possible interactions with anionic lipids and the putative involvement of the positively charged N-terminal extension, we used PA as a representative anionic lipid for additional analyses *in vitro*. We used pull-down assays with immobilized PA (Figure 3C) and a membrane-spotted gradient of PA (Figure 3D) to show that purified AtTSPO binds PA *in vitro*. This interaction required the N-terminal extension, because AtTSPO$^{\Delta N}$ could not bind PA (Figure 3D). We then expressed and purified the N-terminal peptide (first 49 residues) of AtTSPO almost to homogeneity (Figure S5) and compared its capacity to bind PA with that of full-length AtTSPO using thermophoresis (Figure 3E). The N-terminal peptide (AtTSPO^{Nter}) did bind PA, with a similar affinity to full-length AtTSPO (K_d = 2.1 mM for purified AtTSPO and 3.3 mM for the peptide; no statistical difference). These results suggest that the plant-specific N-terminal extension of AtTSPO is responsible for binding to defined anionic lipids *in vitro*, probably via electrostatic/hydrogen bond interactions (Kooijman et al., 2007).

Among PIs that bind to AtTSPO (Figure 3B), we were particularly interested in PI(4,5)P_2, because its roles in ABA signaling, plant osmotic stress responses (Mishra et al., 2006; Lee et al., 2007), and autophagosome initiation and fusion with the lytic compartment (Tan et al., 2016; Baba et al., 2019) indicate possible mechanistic links to autophagic regulation of the stress-induced AtTSPO-PIP2;7 interaction (Hachez et al., 2014). In addition, enzymatic hydrolysis of PI(4,5)P_2 at the plasma membrane can generate secondary signaling lipids such as DAG and PA, which can affect ABA responses (Mishra et al., 2006). Using thermophoresis, we checked whether the N-terminal peptide is required for AtTSPO PI interactions (Figure 4A). Titration of histidine-tagged full-length AtTSPO and truncated AtTSPO$^{\Delta N}$ against a range of PI(4,5)P_2 concentrations revealed a decrease in fluorescence for full-length AtTSPO, indicating binding to PI(4,5)P_2 (Figure 4A). By contrast, no binding was observed with AtTSPO$^{\Delta N}$ (Figure 4A).

Next, we checked whether the purified N-terminus of AtTSPO (AtTSPO^{Nter}) alone was sufficient for interaction with PI(4,5)P_2 (Figure 4B). Lipid overlay experiments showed that both full-length AtTSPO (consistent with previous observations) and its N-terminal peptide could bind PI3P, PI4P, PI5P, and PI(4,5)P_2. By contrast, mTSPO did not bind PI(4,5)P_2, suggesting that the binding determinant for PI(4,5)P_2 is not within the membrane domain of TSPO that is conserved between species. The chimeric mouse TSPO protein (AtTSPO^{Nter}-mTSPO) harboring the plant-specific N-terminal extension could bind PI(4,5)P_2, albeit with reduced affinity compared with full-length AtTSPO or its N-terminal peptide alone (Figure 4C). We used PI3P as a positive control lipid for testing the binding activity of all purified protein variants. Together, these

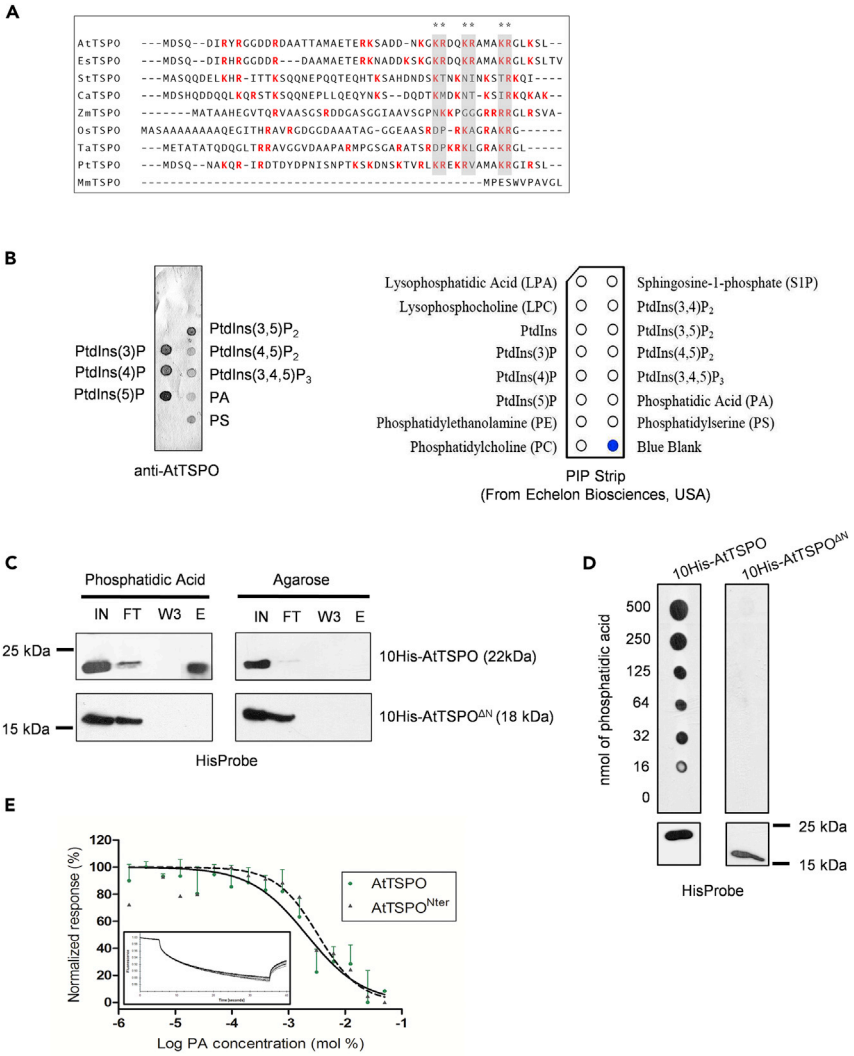

Figure 3. Purified AtTSPO Binds Defined Anionic Lipids *In Vitro* and Binding Requires the N-terminus

(A) The N-terminal extension of plant TSPO is positively charged, as shown by ClustalW alignment of the first 50 residues in higher plant (monocot and dicot) TSPO sequences. At, *Arabidopsis thaliana*; Es, *Eutrema salsugineum*; St, *Solanum tuberosum*; Ca, *Capsicum annuum*; Zm, *Zea mays*; Os, *Oryza sativa*; Ta; *Triticum aestivum*; Pt; *Populus trichocarpa*. Positively charged amino acids are red (neutral pH) and conserved lysine/arginine residues near the transmembrane domain are indicated by gray rectangles. The mouse (*Mus musculus*, Mm) TSPO lacks the plant conserved N-terminal extension.

(B) Initial screening of AtTSPO ligands yielded several candidate anionic lipids. AtTSPO purified from yeast was incubated with spotted lipids in PIP-strip overlay assays (right panel) and detected with anti-AtTSPO antibodies (left panel).

(C) The plant-specific N-terminal extension is involved in AtTSPO-anionic lipid interactions *in vitro*, as shown by lipid-dependent pull-down of AtTSPO. Purified AtTSPO or AtTSPO$^{\Delta N}$[IN] were incubated with PA or agarose resin (negative control). Flow-through [FT], wash (last wash W3), and eluted [E] fractions were probed with HisProbe.

(D) Ten histidine-tagged and N-terminally truncated AtTSPOs expressed and solubilized from yeast microsomes were incubated with a gradient of phosphatidic acid concentrations and detected with HisProbe. The bottom panel shows control detection of both proteins.

(E) Thermophoresis analyses of full-length AtTSPO and its N-terminal peptide titrated against different phosphatidic acid concentrations. Protein samples were labeled with the red fluorescent dye NT-647-NHS, and non-linear fitting of labeled full-length protein (continuous line) yielded a Kd of 2.1 $\pm$ 0.4 mM, compared with a Kd of 3.3 $\pm$ 0.9 mM for the N-terminal peptide (dotted line). The rectangular insert is a representative fluorescence trace. For AtTSPO shown is the mean $\pm$ SD of three experiments and for AtTSPO$^{\Delta N}$ shown is a recorded value from one experiment.

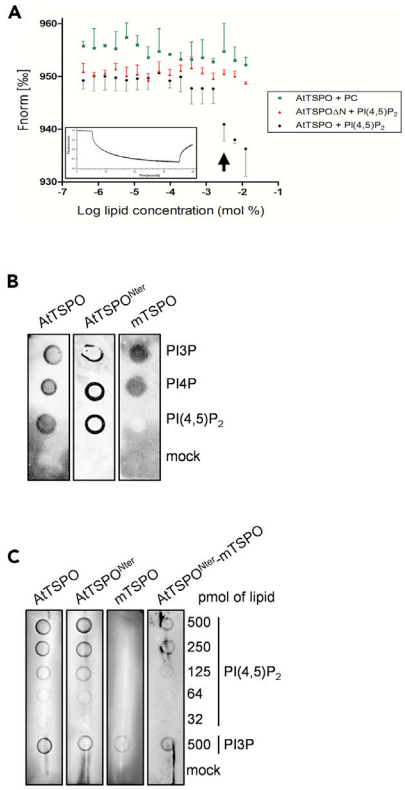

Figure 4. The AtTSPO N-terminal Peptide Binds PI(4,5)P_2

(A) N-terminally truncated AtTSPO cannot bind PI(4,5)P_2 *in vitro*. Thermophoresis was performed by titrating full-length and N-terminally deleted TSPO against different PI(4,5)P_2 concentrations. Protein samples were labeled at polyhistidine tags by RED-tris-NTA. Thermophoretic movement of labeled TSPO increases (normalized fluorescence decreases) upon binding PI(4,5)P_2. Phosphatidylcholine served as a negative control lipid. Both datasets (AtTSPO + PI(4,5)P_2 and AtTSPOΔN + PI(4,5)P_2) were compared using two-way ANOVA followed by Bonferroni multiple comparison post-hoc tests. The threshold lipid concentration yielding statistically significant data ($p < 0.01$) is 1.56 mM (arrow). The non-linear regression-based estimate of the K_d for the AtTSPO-PI(4,5)P_2 interaction is 2.3 $\pm$ 0.7 mM. The rectangular insert is a representative fluorescence trace. For each sample shown is the mean $\pm$ SD of three experiments.

(B) Purified mouse TSPO homolog lacking the plant-specific N-terminus does not bind PI(4,5)P_2 *in vitro*, unlike the full-length plant protein and isolated N-terminal peptide. Five hundred pmol of phosphoinositide was spotted on a nitrocellulose membrane, incubated with purified proteins and detected with anti-AtTSPO (for isolated N-terminus) or HisProbe (for AtTSPO and mTSPO). A mock control of 2% n-dodecyl-β-D-maltoside (DDM) was included.

(C) Chimeric mouse TSPO fused to the AtTSPO N-terminus binds PI(4,5)P_2 *in vitro*. Purified proteins were incubated with different PI(4,5)P_2 concentrations and detected using anti-AtTSPO antibodies (for isolated N-terminal peptide and N-terminus-fused mTSPO) and HisProbe (for AtTSPO and mTSPO). PI3P was spotted as a positive control for mTSPO binding. DDM (2%) served as a mock control. Experiments in (B) and (C) were performed at least twice.

results demonstrate that the plant-specific N-terminus of AtTSPO is a *bona fide* determinant for binding to PI(4,5)P_2 and other PIs.

AtTSPO-mediated Depletion of PI(4,5)P_2 at the PM Requires Its N-terminal Extension

The subcellular distribution of plant PIs is membrane-specific (Kooijman et al., 2007; Hammond et al., 2012; Holthuis and Menon, 2014; Heilmann, 2016; Simon et al., 2014). Under normal growth conditions, PI(4,5)P_2 is mainly localized at the PM in Arabidopsis (Simon et al., 2014), whereas AtTSPO occurs in the ER and mainly in Golgi apparatus (Guillaumot et al., 2009) (Figure S1). To identify where AtTSPO interacts with PI(4,5)P_2 in cells, we used a plant-validated genetically encoded PI(4,5)P_2-specific biosensor (Simon et al., 2014). We first generated stable transgenic Arabidopsis suspension cell lines expressing a double mCherry-tagged phospholipase C PI(4,5)P_2-binding domain under the control of a mild constitutive promoter to limit possible interference with cell physiology. Using ABA treatment to mimic osmotic stress conducive to

AtTSPO expression (Guillaumot et al., 2009; Vanhee et al., 2011a), we observed a partial redistribution of the PI(4,5)P_2 biosensor from the PM to the cytosol, indicating depletion of the free lipid pool in the membrane or concomitant catabolism and/or reduced biosynthesis of PI(4,5)P_2 after ABA treatment (Figure S8).

To investigate whether expression of AtTSPO modified the distribution of PI(4,5)P_2 in cells, we retransformed PI(4,5)P_2 biosensor-expressing cells to constitutively express GFP-tagged AtTSPO or AtTSPO$^{\Delta N}$. Confocal imaging revealed localization of the biosensor at the cell periphery in the absence of AtTSPO, consistent with previous studies showing this construct mainly localized at the PM (Simon et al., 2014) (Figure 5A, upper panels, control cells). Notably, in cells coexpressing GFP-AtTSPO (Figure 5A, middle panels), little or no PI(4,5)P_2 biosensor fluorescence was detected at the cell periphery, but strong fluorescence was seen in mobile punctate structures within cells, colocalized with GFP-AtTSPO in Golgi stacks, because GFP-AtTSPO is mainly localized in Golgi membranes (Guillaumot et al., 2009). By contrast, coexpressing the truncated form of AtTSPO (GFP-AtTSPO$^{\Delta N}$), which also localizes to Golgi membranes, had no distinct effect on biosensor distribution (Figure 5A, bottom panels; see also Figure S2E). GFP fluorescence from both full-length and truncated AtTSPO was detected in cell vacuoles (asterisks), suggesting truncation of the plant-specific N-terminus did not preclude AtTSPO targeting to and degradation in the vacuole.

To ascertain whether expression of AtTSPO decreases PI(4,5)P_2 levels at the PM, we prepared PM-enriched fractions from cell lines and performed dot blot experiments to measure relative PI(4,5)P_2 content with antibody specific for this lipid (Yakir-Tamang and Gerst, 2009) (Figure 5B) and anti-H^+-ATPase (PMA) to normalize the quantified signal. As expected, AtTSPO expression decreased PI(4,5)P_2 levels by ~ two-thirds, whereas PI(4,5)P_2 was decreased by ~23% when N-terminally truncated AtTSPO was expressed (Figure 5B). These results suggest that the plant-specific N-terminus is required for efficient AtTSPO-induced depletion of PI(4,5)P_2 from the PM and its concomitant enrichment and colocalization with AtTSPO in Golgi membranes.

Because the biosynthesis of PI(4,5)P_2 is catalyzed by PI4P 5-kinase at the PM via phosphorylation of PI4P (Kooijman et al., 2007; Ischebeck et al., 2008; Hammond et al., 2012; Holthuis and Menon, 2014; Heilmann, 2016), AtTSPO-induced accumulation of PI(4,5)P_2 in Golgi membranes may be linked to enrichment of PI4P 5-kinase and relatively low levels of PI4P present in the Golgi compartment (Simon et al., 2014). We transiently expressed the mCherry-tagged human PI4P 5-kinase (mCherry-HsPIPK1α) fusion protein known to be active in plant cells (Ischebeck et al., 2008; Ischebeck et al., 2011) and compared its localization in WT tobacco and plants stably expressing YFP-AtTSPO. No difference in kinase subcellular localization was observed, suggesting that the trafficking of expressed mCherry-HsPIPK1α in the plant cell is not detectably affected by AtTSPO expression (Figure S9). Phosphoinositide-specific PLC (PI-PLC) and non-specific PLC (NPC) family lipases have been implicated in ABA signaling and salt and drought stress (Lee and Assmann, 1991; Hirayama et al., 1995; Sanchez and Chua, 2001;Hunt et al., 2003; Im et al., 2007; Peters et al., 2010), conditions conducive to AtTSPO induction. During receptor-regulated PLC signaling in animal cells, PI(4,5)P_2 levels can drop rapidly at the PM (Peters et al., 2010.; Yen et al., 2018). We wondered whether expression of AtTSPO in plant seedlings with or without additional ABA treatment could modify PLC activity. As shown in Figure 5C (black histograms), control seedlings (without ABA treatment) overexpressing AtTSPO (OE TSPO) displayed ~25% more PLC activity than WT seedlings. By comparison, seedlings lacking AtTSPO (KO TSPO) or overexpressing N-terminally truncated AtTSPO (OE TSPO[ΔN]) exhibited similar PLC activities (~50% that of WT seedlings). Preincubation of seedlings in ABA marginally enhanced PLC activity in WT seedlings (~20% compared with untreated samples) but dramatically increased activity in OE TSPO seedlings (~4-fold), suggesting the effect of AtTSPO on PLC activity is enhanced by ABA signaling. Interestingly, ABA treatment had no effect on PLC activity in KO TSPO seedlings or transgenic seedlings overexpressing N-terminally truncated AtTSPO. These results suggest that PLC activity at the PM is modulated by ABA signaling and TSPO expression in plants, and TSPO-dependent enhancement of PLC activity requires the plant-specific N-terminal polybasic extension.

Lysine/Arginine Pairs in the N-terminal Extension of AtTSPO Are Required for Both PI(4,5)P_2 Binding and Interaction with Aquaporin PIP2;7 *In Vivo*

To identify key amino acids in the N-terminus of AtTSPO involved in interactions with PI(4,5)P_2, we performed NMR analysis of the purified N-terminus (first 50 amino acids) labeled with ^{5}N and ^{13}C (Figure S5). The very good spectral quality of the purified N-terminal construct (Figure 6A) allowed effective recording of 2D and triple resonance 3D data, facilitating full ^{1}H, ^{15}N, and ^{13}C assignments. Chemical shift analysis

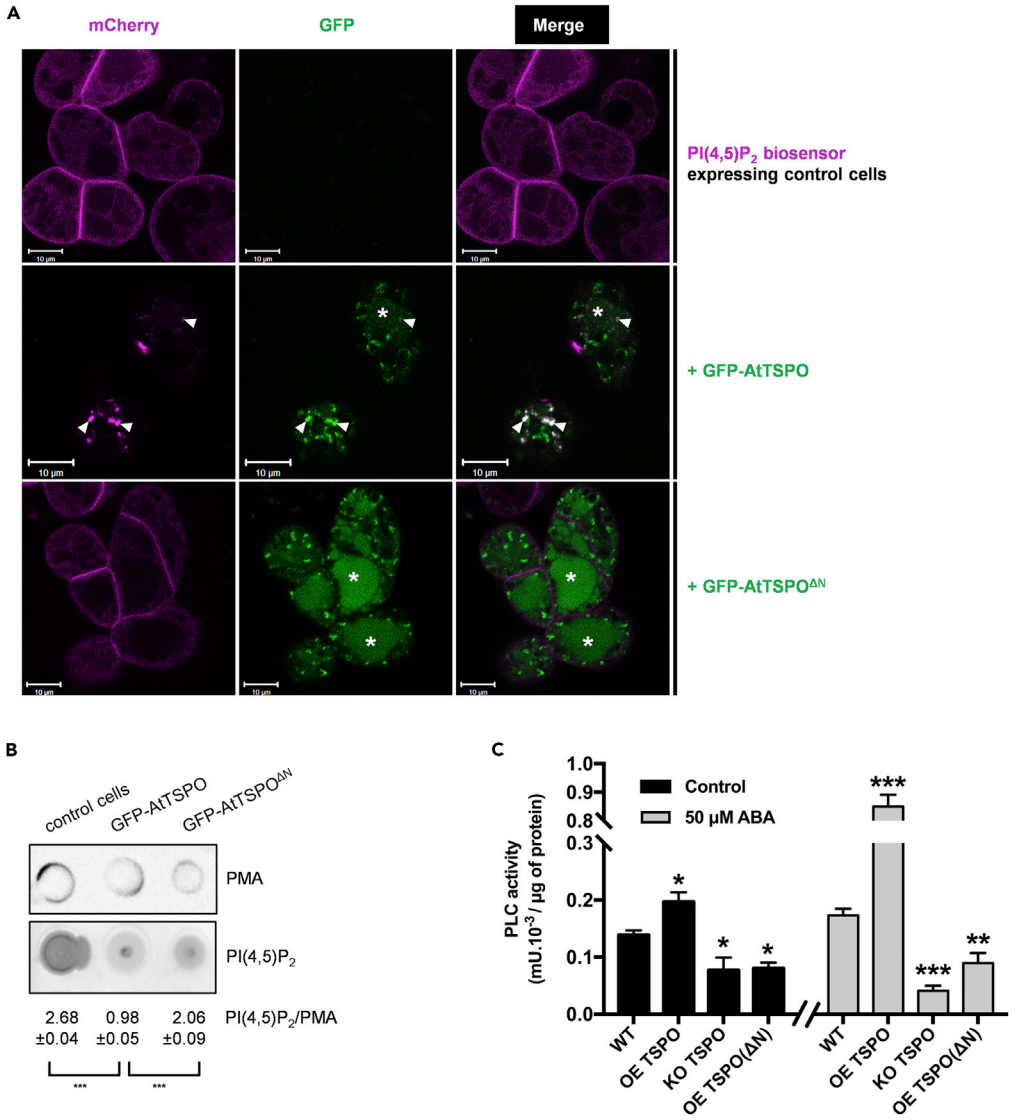

Figure 5. PI(4,5)P_2 Biosensor Was Depleted from the PM and Partially Colocalized with AtTSPO in Golgi Membranes in the Presence of Full-length AtTSPO but Not AtTSPO$^{\Delta N}$

(A) Representative confocal images of Arabidopsis suspension cells stably coexpressing the PI(4,5)P_2biosensor (mCherry-tagged double pleckstrin homology domain from phospholipase C; magenta) and full-length AtTSPO or AtTSPO$^{\Delta N}$ (GFP-tagged; green). Arrowheads indicate mCherry and GFP signals colocalizing at Golgi membranes. * indicates GFP fluorescence in the vacuole. Bars = 10 µm.

(B) Solubilized PM-enriched fractions from cells imaged as in (A) were spotted on a nitrocellulose membrane, and PI(4,5)P_2 was detected using monoclonal anti-PI(4,5)P_2 antibodies. For signal quantification (ImageJ 1.51 software) we used PM proton ATPase (PMA) as a control.

(C) Ten-day-old Arabidopsis seedlings grown on MS agar plates were incubated in liquid MS medium with or without 50 µM ABA for 24 h, and PLC activity was measured in triplicate using an EnzCheck direct phospholipase C assay kit. Statistical significance was analyzed by one-way ANOVA followed by Tukey's test (***$p < 0.001$; **$p < 0.01$; *$p < 0.05$). Data in (B) and (C) are means ± SD from three technical replicates, and all experiments were performed at least twice.

suggested the peptide was poorly structured and did not adopt a stable globular fold. Calculation of secondary structure propensity (SSP) (Marsh et al., 2006) revealed that two regions (R14-R26 and D31-K44) had a tendency to form α-helices (Figure 6B). The N-terminal peptide showed no interaction with calcium or zwitterionic lipids such as dimyristoylphosphatidylcholine (DMPC) bicelles, but it interacted with negatively charged dimyristoylphosphatidylglycerol bicelles, according to heteronuclear single quantum coherence

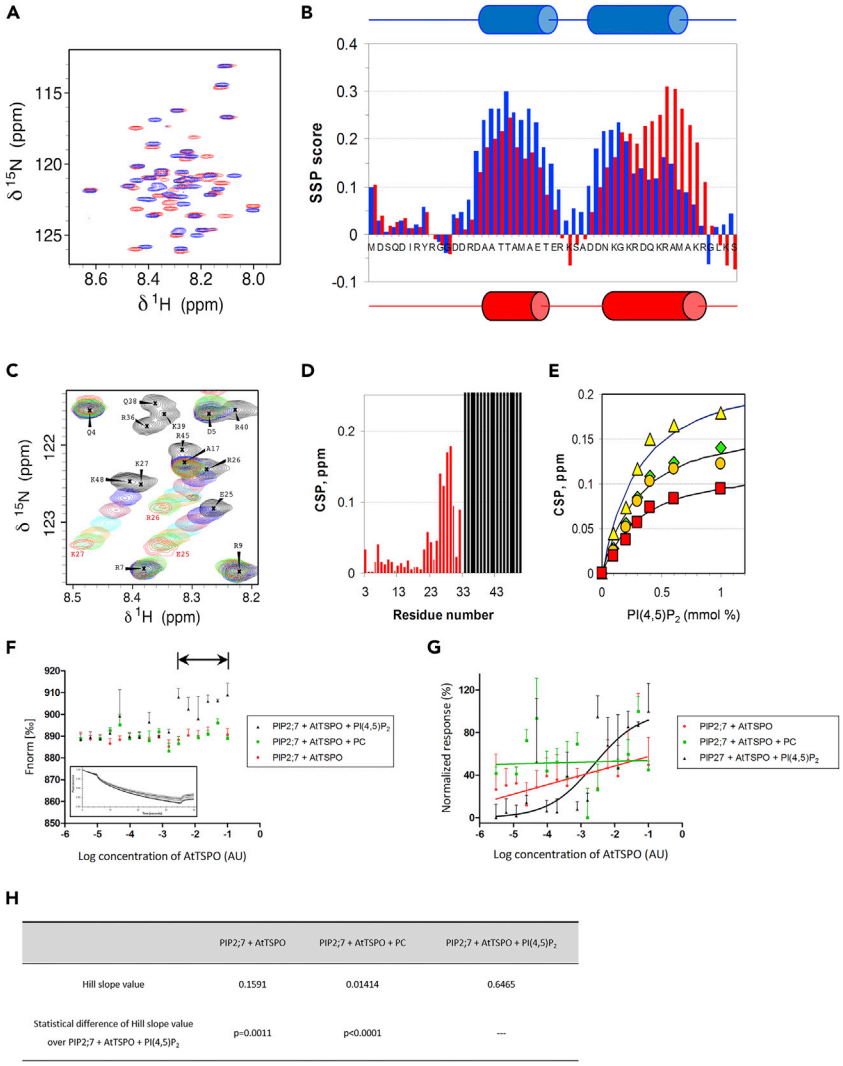

	PIP2;7 + AtTSPO	PIP2;7 + AtTSPO + PC	PIP2;7 + AtTSPO + PI(4,5)P_2
Hill slope value	0.1591	0.01414	0.6465
Statistical difference of Hill slope value over PIP2;7 + AtTSPO + PI(4,5)P_2	p=0.0011	p<0.0001	---

Figure 6. The Recombinant AtTSPO N-terminal Peptide Interacts with PI(4,5)P_2 and This Anionic Lipid Is Required for AtTSPO Interaction with the Aquaporin PIP2;7 *In Vitro*

(A) 2D ^{1}H-^{15}N HSQC spectrum (500 MHz, 30°C) of 100 μM AtTSPO^{Nter} in the absence (blue) and in the presence (red) of 25 mM DMPG/50 mM DHPC bicelles.

(B) Secondary Structure Propensity (SSP) score in the absence (blue) and in the presence (red) of DMPG/DHPC bicelles.

(C) Selected region in 2D ^{1}H-^{15}N HSQC showing different behaviors of residues upon titration of AtTSPO^{Nter} with increasing amounts of PI(4,5)P_2 (0 mM, black; 0.1 mM, blue; 0.2 mM, maroon; 0.3 mM, cyan; 0.4 mM, orange; 0.6 mM, green; 1 mM, red). Residues R36, Q38, K39, R40, and K48 disappear at the first addition of PI(4,5)P_2, whereas residues E25, R26, and K27 show progressive chemical shift perturbations.

(D) ^{1}H,^{15}N Chemical Shift Perturbations (CSP) after addition of 1 mM PI(4,5)P_2. Residues 34–49 that disappear at the first point of the titration are indicated by gray shading. CSPs were calculated as $|\Delta\delta(^{1}H)| + |\Delta\delta(^{15}N)|/10$.

(E) CSP of E26 (green diamonds), R27 (orange circles), K28 (yellow triangles), and A30 (red squares) as a function of PI(4,5)P_2 concentration added.

(F) Thermophoresis analyses of YFP-PIP2;7 titrated against different AtTSPO concentrations. PIP2;7 movement was followed by YFP fluorescence. Either 50 μM PI(4,5)P_2, phosphatidylcholine (PC, negative control), or no lipid was added. Thermophoretic motion of Venus-PIP2;7 decreases (normalized fluorescence increases) upon binding of AtTSPO in the presence of 50 μM PI(4,5)P_2 but not PC, nor in the absence of lipids. The horizontal arrow indicates the bound state plateau region. The rectangular insert is a representative fluorescence trace. For each sample shown is the mean ± SD of three experiments.

(G) Data from (F) were normalized and fitted using non-linear regression, yielding a typical sigmoidal binding curve only in the presence of PI(4,5)P_2.

(H) Statistical comparison of Hill slope values from (G). Low pvalues indicate no similarity in steepness between fitted curves.

spectroscopy (HSQC) spectra (Figure 6A), leading to increased stabilization of the C-terminal R36-R45 helical segment (Figure 6B). Titration of the peptide with $PI(4,5)P_2$ micelles induced larger changes in ^{1}H-^{15}N HSQC spectra than did DMPG bicelles (Figures 6A and 6C), suggesting stronger interactions with $PI(4,5)P_2$. H-^{15}N cross-peaks of residues belonging to the 34–49 segment completely disappeared (Figure 6C), indicating a tight association between the C-terminal region of the peptide and $PI(4,5)P_2$. Other residues along 20–32 segment exhibited a progressive chemical shift variation upon titration corresponding to fast exchange (Figures 6C and 6D). Monitoring these chemical shift perturbations during titration (Figure 6D) allowed estimation of a K_d in the range of 0.15 mM for the interaction between these residues and $PI(4,5)P_2$.

To confirm that $PI(4,5)P_2$ is required for AtTSPO-PIP2;7 interactions, we used thermophoresis to monitor the contribution of $PI(4,5)P_2$ to the interaction *in vitro* (Figures 6F and 6G). We used a transgenic line expressing Venus-PIP2;7 (Hachez et al., 2014) to solubilize the protein from the microsomal fraction and titrated it against different AtTSPO concentrations in the presence and absence of $PI(4,5)P_2$ in trans. As shown in Figures 6F and 6G, there was no interaction between AtTSPO and Venus-PIP2;7 in the absence of $PI(4,5)P_2$ or in the presence of 50 μM phosphatidylcholine. By contrast, in the presence of 50 μM $PI(4,5)P_2$, Venus-PIP2;7 fluorescence increased, generating a double plateau pattern, clearly indicating a protein-protein interaction. Indeed, a non-linear regression model for binding could only be fitted in the presence of $PI(4,5)P_2$ (Figures 6G and 6H). Thus, AtTSPO-PIP2;7 interactions are modulated by $PI(4,5)P_2$.

$PI(4,5)P_2$ Mediates AtTSPO-PIP2;7 Interactions *In Vivo*

Analysis of the N-terminal extension of AtTSPO revealed several key amino acids potentially interacting with $PI(4,5)P_2$, and the C-terminal region of the peptide was most affected upon interaction. Interestingly, this segment contains three positively charged lysine/arginine pairs—K35-R36, K39-R40, and K44-R45—that may contribute to the interaction (Figures 3A and 6C). To test whether interaction with $PI(4,5)P_2$ is required for AtTSPO to interact with PIP2;7, we generated point substitutions of these residue pairs and tested binding strength to PIP2;7 by BiFC. Double substitution mutants $AtTSPO^{K35A/R36A}$ and $AtTSPO^{K39A/R40A}$ and quadruple mutant $AtTSPO^{K39A/R40A/K44A/R45A}$ (Figure 7) were generated. A Golgi-localized xylosyltransferase tagged with the monomeric variant of a cyan fluorescent protein (mTurquoise) was used as a transfection control (Gookin and Assmann, 2014) and for both colocalization and normalization of the BiFC signal (Figure S3). As expected, coexpression of WT AtTSPO and PIP2;7 generated a mainly Golgi-localized BiFC signal (Figure 7A, upper panels, arrowheads). Notably, all tested mutant combinations yielded substantially lower BiFC signals (Figure 7A), less than 20% that of the WT protein (Figure 7B). These results suggest that mutations affecting $PI(4,5)P_2$ binding to the N-terminus of AtTSPO also reduced the efficiency of its interaction with aquaporin PIP2;7 *in vivo*.

DISCUSSION

Herein, we investigated the potential physiological role and evolutionary significance of the N-terminal extension in plant TSPO. We demonstrate that stress-induced plant TSPO protects plant tissues against water loss by depleting the PM of a major water channel and the signaling lipid $PI(4,5)P_2$. These functions require the plant-specific polybasic N-terminus absent in bacterial and animal TSPO. We provide evidence suggesting a molecular link between Arabidopsis AtTSPO, $PI(4,5)P_2$, and the highly expressed PM aquaporin PIP2;7 that underpins responses to dehydration. Additionally, the findings reveal cell-type-dependent functional evolution among TSPOs.

Involvement in stress responses appears to be a common feature among TSPOs across kingdoms (Vanhee et al., 2011a; Batoko et al., 2015; Li et al., 2016; Guilarte et al., 2016), but the molecular mechanism and cellular components are yet to be described in any cell type. Herein, we show that AtTSPO reduces aquaporin PIP2;7 levels at the cell surface to reduce water loss, and this function requires the plant-specific N-terminal extension of AtTSPO. Interestingly, expressing the mouse mitochondrial TSPO homolog (mTSPO) in plant cells did not affect PIP2;7 levels, but a chimeric version ($AtTSPO^{Nter}$-mTSPO) containing the plant-specific N-terminus of AtTSPO did lower PIP2;7 abundance at the PM. Thus, acquisition of the conserved N-terminal extension through evolution has endowed plant TSPO with unique cellular responses and adaptation to osmotic stress.

The AtTSPO N-terminal extension binds the signaling lipid $PI(4,5)P_2$ *in vitro* and *in vivo*, and this may be a prerequisite for physical and functional interactions with aquaporin PIP2;7. Cells expressing AtTSPO accumulated a $PI(4,5)P_2$ biosensor at the Golgi membrane rather than the PM, as did control cells and cells

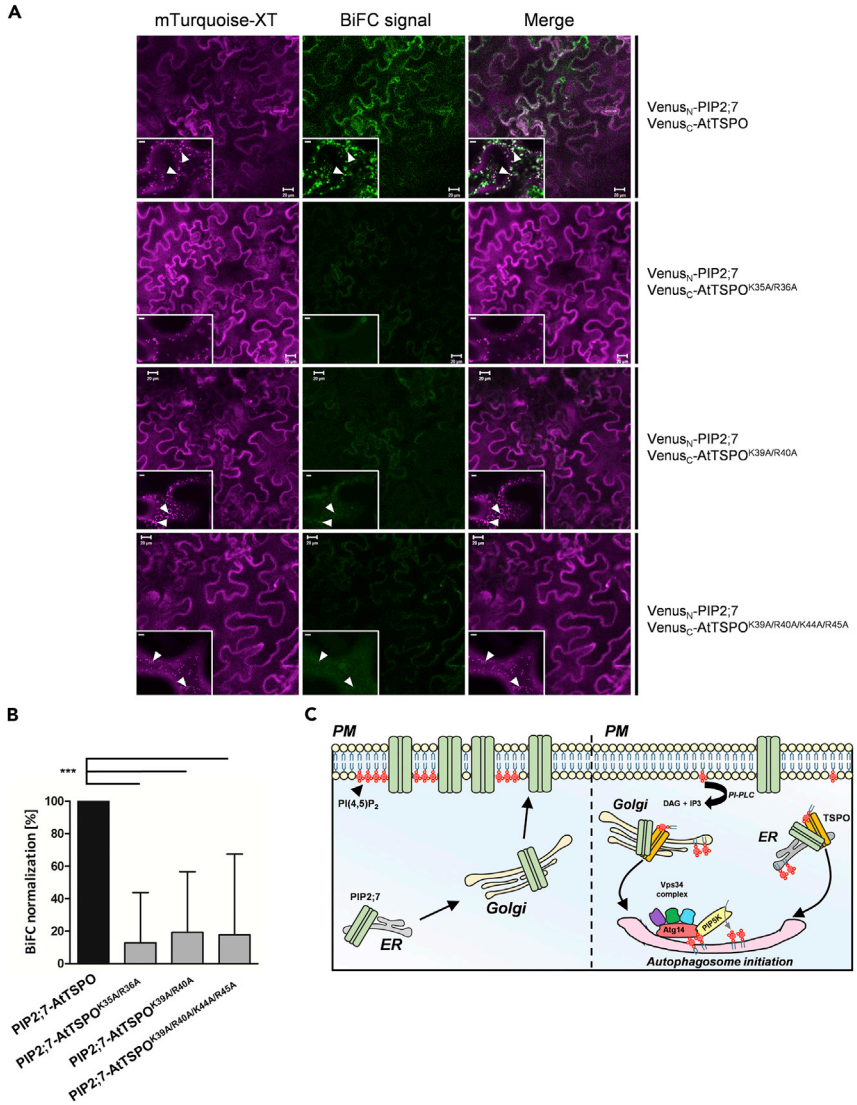

Figure 7. Specific Positively Charged Lysine-Arginine Pairs in the N-terminal Region of AtTSPO Mediate Interaction with PIP2;7 *In Vivo*

(A) Representative confocal images of tobacco epidermal cells transiently coexpressing $Venus_N$-PIP2;7 and $Venus_C$-AtTSPO or $Venus_N$-PIP2;7 and $Venus_C$-AtTSPO point mutants. Xylosyltransferase-mTurquoise fluorescent chimera (magenta) served as a cell transfection control (Golgi marker) and for signal quantification. Full-length PIP2;7 and AtTSPO served as a positive control for the BiFC signal. Low-magnification images qualitatively demonstrate the occurrence and distribution of BiFC (green) in the transfected area, and insets of high-magnification images show Golgi stacks (arrowheads). For PIP2;7-AtTSPO$^{K35A/R36A}$, colocalization of the BiFC signal and Golgi marker was not detected. Bars = 20 μm and 5 μm for low and high magnification, respectively. Experiments were repeated three times.

(B) Signal quantification showing a drastic reduction in BIFC between PIP2;7 and AtTSPO mutants compared with full-length AtTSPO. Statistical analysis was based on one-way ANOVA followed by Tukey's tests (***$p < 0.001$). Bars represent means +/− SD. See transparent methods section for quantification procedure.

(C) Hypothetical model of $PI(4,5)P_2$-dependent PIP2;7 downregulation by AtTSPO during stress. Under normal conditions (left), synthesized PiP2;7 is targeted to the PM through the biosynthetic secretory pathway. Under osmotic stress conditions (right), expressed AtTSPO is targeted to the ER and Golgi membranes.AtTSPO stimulates PLC activity, depleting $PI(4,5)P_2$ at the PM and generating DAG and PA that modulate the activity of PP2C phosphatases involved in ABA-dependent reduction of water loss through stomata. Decreased $PI(4,5)P_2$ at the PM prevents recruitment of PIP2;7-containing vesicles. Golgi/ER-localized AtTSPO binds $PI(4,5)P_2$ synthesized *de novo* in these compartments, inducing structural changes needed for recognition and interaction with PIP2;7 *en route* to the PM, causing redirection to nascent autophagosomes. AtTSPO cannot directly deplete $PI(4,5)P_2$ from the PM but may form a protein complex that recruits

Figure 7. *Continued*

PIP5K to organelle/autophagosome initiation sites. AtTSPO-mediated enrichment of ER/Golgi membranes with PI(4,5)P_2 may initiate autophagy. Autophagosomal membranes also recruit PIP5K that generates PI(4,5)P_2 and the autophagy regulator Atg14/Barkor that interacts with both the enzyme and PI(4,5)P_2. PI(4,5)P_2 binding to Atg14 regulates its interaction with the Vps34 complex catalyzing PI3P synthesis at autophagosome initiation sites. The presence of the AtTSPO-PI(4,5)P_2-PIP2;7 complex in ER/Golgi membranes and the phagophore containing PI(4,5)P_2 and Atg8 may be close enough to allow lipid-protein and protein-protein interactions.

expressing a truncated version of AtTSPO devoid of its N-terminal extension. Thus, in the presence of AtTSPO, Golgi membranes become enriched in free PI(4,5)P_2, possibly at the expense of the PM. We did not find any significant difference in overall PM levels between cells expressing AtTSPO and control cells (Figure S11), but PI(4,5)P_2 depletion was specifically observed in PM fractions from cells expressing AtTSPO compared with controls and cells expressing N-terminally truncated AtTSPO (Figure 5B). This suggest that expression of AtTSPO has a target effect on PM PI(4,5)P_2 levels. Phospholipid transport proteins function at organelle contact sites (Wang et al., 2014, 2019; Yen et al., 2018). Transient apposition between organelles can alter PI levels by presenting membrane-bound phosphatases and/or phosphoinositide-specific transporters to their respective substrates (Wang et al., 2019). Recent studies identified proteins mediating PI(4,5)P_2 removal from the PM of eukaryotic cells (Cockcroft and Raghu, 2018; Wang et al., 2019), but whether AtTSPO is enriched in organelle contact sites and/or whether it transports lipid molecules remains unknown. Biosensor experiments demonstrated a substantial amount of free PI4P in the PM of plant cells expressing AtTSPO, suggesting PI(4,5)P_2 depletion in the presence of AtTSPO may reflect mislocalization or inhibition of PM-bound PI4P5K enzyme activity. However, AtTSPO did not affect subcellular localization of a functional heterologously expressed PI4P5K (Figure S9). We cannot exclude the possibility that endogenous plant PIP5K may act differently and AtTSPO may affect its localization resulting in PI(4,5)P_2 remodeling. So far, we have no evidence suggesting that AtTSPO is involved directly in the translocation of any of its lipid ligand and whether any of these interactions could modulate the structure-function of AtTSPO. We favor the possibility that expression of AtTSPO induces the enrichment of PI(4,5)P_2 in the Golgi membrane by enhancing the enzymatic phosphorylation of its precursor PI4P within this lipid bilayer.

Phosphatase-mediated hydrolysis of PI(4,5)P_2 generates second messengers such as DAG and PA involved in ABA signaling. Expression of AtTSPO stimulates PLC activity. Because the kit used to measure this activity does not specifically report on PI-PLC, it may be that expression of AtTSPO enhances PLC in general, including NPC activity. It was shown that overexpression of NPC4 renders plants more sensitive to ABA and more tolerant to hyperosmotic stress than WT plants (Peters et al., 2010). NPC-produced DAG is converted to PA, and its derived lipids positively modulate ABA response and promote plant tolerance to drought and salt stresses. Interestingly, the ABA-dependent increase in PLC activity requires full-length AtTSPO (Figure 5C), suggesting that ABA may alter PM levels of PI(4,5)P_2 via plant TSPO. Both PI-PLC and NPC promote responses to ABA and tolerance to hyperosmotic stress, but there is no evidence of protein kinase C enzymes or inositol triphosphate (IP3) receptors in plants. PLC-dependent signaling is essentially mediated by PA generated from DAG by DAG kinase (Hong et al., 2016). PA effector proteins in plants include ABI1, an ABA co-receptor protein and negative regulator of this stress hormone-signalling pathway, and the Gα subunit of heterotrimeric G protein. This relates to opening of stomata and water loss, because binding to ABI1 promotes stomatal closure and Gα binding to PA mediates ABA inhibition of stomatal opening (Mishra et al., 2006). Interestingly, stress- and ABA-dependent induction of AtTSPO is highest in guard cells. Circumstantial evidence (Ma et al., 2015) suggests a positive correlation between PI(4,5)P_2 abundance in the PM, increased active aquaporins, and increased osmotic water permeability. Consistently, AtTSPO expression reduced levels of both PI(4,5)P_2 and PIP2;7 at the PM and reduced water loss in transgenic plants expressing AtTSPO or its stabilized point mutant AtTSPO^{H91A}, compared with WT plants. It is not yet known whether PI(4,5)P_2 directly or indirectly modulates the structure-function properties of PM aquaporins, although other channels responding to osmotic stress are regulated by PI(4,5)P_2 (Liu et al., 2005).

Free PI(4,5)P_2 is normally found in the PM, as demonstrated by cognate biosensor subcellular localization and biochemical analyses (Simon et al., 2014). Whether PI(4,5)P_2 signaling occurs in intracellular compartments of eukaryotic cells remains contentious, although evidence supports specific and essential functions for intracellular PI(4,5)P_2 (Tan et al., 2015). Levels of PI(4,5)P_2 in intracellular compartments are low, presumably due to lack of free PI(4,5)P_2, which is bound to effectors associated with biosynthetic kinases (PI4P5Ks).

The present work suggests that AtTSPO expression triggers accumulation of free $PI(4,5)P_2$ at the Golgi membrane, but exactly how this intracellular $PI(4,5)P_2$ signaling platform is generated remains unclear. The effect of expressed AtTSPO on the relative level of PIP2;7 at the PM could indirectly also affect the level of $PI(4,5)P_2$ in addition to enhancing PLC activity. It may be that induction of AtTSPO at Golgi/ER binds PIP2;7 and prevents it from reaching the PM. The lack of the aquaporin at the PM may affect PI(4,5)2 levels along with other effects of the osmotic stress on PLC or PIP5K activity.

Generation of $PI(4,5)P_2$ requires recruitment of PIP kinases, particularly PI4P5Ks, to the target membrane, typically via the same effectors that bind $PI(4,5)P_2$. In addition to PI3P and PI5P, $PI(4,5)P_2$ contributes to initiation, trafficking of membrane precursors, and fusion of autophagosomes with the lytic compartment (Tan et al., 2016). Nucleation of the autophagosome initiation membrane requires the vacuolar protein sorting (VPS) 34 complex, which generates PI3P. The VPS34 complex is recruited to autophagosome initiation sites by ATG14/Barkor, which binds PI3P via a Barkor/ATG14 autophagosome-targeting sequence (BATS) domain, and this domain also binds PI4P5K and $PI(4,5)P_2$ (Tan et al., 2016). $PI(4,5)P_2$ signaling at autophagosome initiation membranes could facilitate targeting of the AtTSPO containing complex to this site. Binding of $PI(4,5)P_2$ was not required for autophagy-dependent degradation of AtTSPO, because the N-terminally truncated protein cannot bind $PI(4,5)P_2$ but was still translocated to the vacuole (Figure 5A). However, binding of $PI(4,5)P_2$ is necessary for AtTSPO to interact with aquaporin PIP2;7. This interaction could occur because autophagosomes are initiated near AtTSPO-containing organelles, allowing the cytosolic N-terminus of AtTSPO to contact the autophagosome initiation membrane enriched in $PI(4,5)P_2$ and PI3P (Figure 7C). How exactly the AtTSPO-containing complex is extracted and translocated to the autophagosomal membrane remains unknown.

Structural analysis suggests that lipid binding by the N-terminal extension of AtTSPO may induce protein conformational changes. Interaction with anionic lipids stabilized helical structure within the 34–49 segment, close to the first transmembrane region of AtTSPO. Conformational changes induced by $PI(4,5)P_2$ binding may therefore expose residues that interact with PIP2;7 within the lipid bilayer. The 34–49 segment contains key arginine/lysine residues involved in $PI(4,5)P_2$ binding *in vitro*, and their mutation dramatically decreased AtTSPO interaction with PIP2;7 *in vivo*.

In conclusion, in response to osmotic stress, Arabidopsis TSPO is induced at the Golgi membrane, triggering depletion of $PI(4,5)P_2$ at the PM and its subsequent enrichment at the Golgi membrane. Moreover, AtTSPO binds $PI(4,5)P_2$ via its polybasic plant-specific N-terminus as a requirement for its interaction with the PM aquaporin PIP2;7. Given its involvement in key cellular processes at the PM, mechanisms controlling the localization and/or abundance of the multifunctional $PI(4,5)P_2$ at the PM are of great interest for understanding cellular signaling and its implications. This work demonstrates how stress causes $PI(4,5)P_2$ remodeling through expression of plant TSPO.

This underlying molecular mechanism illuminates functional divergence among TSPOs; the plant-specific N-terminal extension rich in polybasic residues determines the involvement of TSPO in osmotic stress responses.

Limitations of the Study

We found that both AtTSPO and the mouse TSPO bind PI3P *in vitro*. However, it is not clear yet whether this observation could be extended to bacterial TSPO, in which case it would be interesting to investigate if this has any conserved physiological meaning *in vivo*. The role of AtTSPO in osmotic response is intriguing and could be analyzed further in a cell-type-dependent manner, for example by expressing the relatively stable mutant variant of AtTSPO in the guard cells. It will be equally interesting to know if there is difference in the composition of the lipid at the PM vs the punctate structures enriched in AtTSPO or if different PIP5Ks are activated at this location.

METHODS

All methods can be found in the accompanying Transparent Methods supplemental file.

SUPPLEMENTAL INFORMATION

Supplemental Information can be found online at https://doi.org/10.1016/j.isci.2020.100889.

ACKNOWLEDGMENTS

We thank M. Boutry (LIBST, UCLouvain, Belgium) for sharing purified TEV enzyme and anti-PMA antibodies, M. Ghislain (LIBST, UCLouvain, Belgium) for anti-FLAG antibodies, K. Moonens (VIB, Center for Structural Biology, VUB, Belgium) for assistance with MST, D. Masquelier for preparing AtTSPO^{Nter}-mTSPO, and A. Jurkiewicz, J. Nader, and M.C. Eloy for technical assistance. We acknowledge Y. Jaillais (Laboratoire Reproduction et Développement des Plantes, ENS Lyon, France), T. Munnik (Swammerdam Institute for Life Sciences, University of Amsterdam, The Netherlands), S. Assmann (Department of Biology, Pennsylvania State University, USA), and I. Heilmann (Institute for Biochemistry and Biotechnology, Martin-Luther-University Halle-Wittenberg) for providing reagents and genetic materials. Transgenic Arabidopsis plants expressing mVenus-AtTSPO$^{\Delta N}$ were generated by S. Guillon (UCLouvain). SL received a PhD fellowship from the Ministère de la Recherche Française. PJ received a PhD fellowship from UCLouvain-FSR. HA received a PhD fellowship from UCLouvain-ADRI. This work was partly funded by the Wallonia-Brussels Federation Joint Research Action (ARCgrant#11/16-036 to H.B.), and the Belgian Funds for Scientific Research (FNRS; CR grant#19516174 and PDRgrant# 6794930 and T.0050.18 to H.B.). H.B. is a senior research associate of FRS-FNRS.

AUTHOR CONTRIBUTIONS

Conceptualization: O.L, J.-J.L, and H.B.; Methodology and Investigation, P.J., L.S., H.A., O.L., J.-J.L., and H.B.; Writing—Original Draft, P.J., J.-J.L., and H.B.; Review & Editing, P.J., O.L., J.-J.L., and H.B.; Funding Acquisition J.-J.L. and H.B.; Supervision, J.-J.L. and H.B.

DECLARATION OF INTERESTS

The authors have no conflict of interest to declare.

Received: June 21, 2019
Revised: November 30, 2019
Accepted: February 3, 2020
Published: March 27, 2020

REFERENCES

Augustine, J.J., Bodziak, K.A., and Hricik, D.E. (2007). Use of sirolimus in solid organ transplantation. Drugs *67*, 369–391.

Baba, T., Toth, D.J., Sengupta, N., Kim, Y.J., and Balla, T. (2019). Phosphatidylinositol 4,5bisphosphate controls Rab7 and PLEKMH1 membrane cycling during autophagosome lysosome fusion. EMBO J. *38*, e102837.

Bae, K.R., Shim, H.J., Balu, D., Kim, S.R., and Yu, S.W. (2014). Translocator protein 18 kDa negatively regulates inflammation in microglia. J. Neuroimmune Pharmacol. *9*, 424–437.

Banati, R.B., Middleton, R.J., Chan, R., Hatty, C.R., Kam, W.W., Quin, C., Graeber, M.B., Parmar, A., Zahra, D., Callaghan, P., et al. (2014). Positron emission tomography and functional characterization of a complete PBR/TSPO knockout. Nat. Commun. *5*, 5452.

Batoko, H., Veljanovski, V., and Jurkiewicz, P. (2015). Enigmatic Translocator protein (TSPO) and cellular stress regulation. Trends Biochem. Sci. *40*, 497–503.

Braestrup, C., and Squires, R.F. (1977). Specific benzodiazepine receptors in rat brain characterized by high-affinity (3H)diazepam binding. Proc. Natl. Acad. Sci. U S A *74*, 3805–3809.

Cockcroft, S., and Raghu, P. (2018). Phospholipid transport protein function at organelle contact sites. Curr. Opin. Cell Biol. *53*, 52–60.

Cutler, S.R., Rodriguez, P.L., Finkelstein, R.R., and Abrams, S.R. (2010). Abscisic acid: emergence of a core signaling network. Annu. Rev. Plant Biol. *61*, 651–679.

Davey, M.E., and de Bruijn, F.J. (2000). A homologue of the tryptophan-rich sensory protein TspO and FixL regulate a novel nutrient deprivation-induced Sinorhizobium meliloti locus. Appl. Environ.Microbiol. *66*, 5353–5359.

Doi, A., Fujimoto, A., Sato, S., Uno, T., Kanda, Y., Asami, K., Tanaka, Y., Kita, A., Satoh, R., and Sugiura, R. (2015). Chemical genomics approach to identify genes associated with sensitivity to rapamycin in the fission yeast Schizosaccharomyces pombe. Genes Cells *20*, 292309.

Fan, J., Lindemann, P., Feuilloley, M.G., and Papadopoulos, V. (2012). Structural and functional evolution of the translocator protein (18 kDa). Curr. Mol. Med. *12*, 369–386.

Gatliff, J., East, D., Crosby, J., Abeti, R., Harvey, R., Craigen, W., Parker, P., and Campanella, M. (2014). TSPO interacts with VDAC1 and triggers a ROS-mediated inhibition of mitochondrial quality control. Autophagy *10*, 2279–2296.

Gatliff, J., East, D.A., Singh, A., Alvarez, M.S., Frison, M., Matic, I., Ferraina, C., Sampson, N., Turkheimer, F., and Campanella, M. (2017). A role for TSPO in mitochondrial Ca. Cell Death Dis. *8*, e2896.

Gookin, T.E., and Assmann, S.M. (2014). Significant reduction of BiFC non-specific assembly facilitates in planta assessment of heterotrimeric G-protein interactors. Plant J. *80*, 553–567.

Guilarte, T.R., Loth, M.K., and Guariglia, S.R. (2016). TSPO finds NOX2 in microglia for redox homeostasis. Trends Pharmacol. Sci. *37*, 334–343.

Guillaumot, D., Guillon, S., Déplanque, T., Vanhee, C., Gumy, C., Masquelier, D., Morsomme, P., and Batoko, H. (2009). The Arabidopsis TSPO-related protein is a stress and abscisic acidregulated, endoplasmic reticulum-Golgi-localized membrane protein. Plant J. *60*, 242–256.

Guo, Y., Kalathur, R.C., Liu, Q., Kloss, B., Bruni, R., Ginter, C., Kloppmann, E., Rost, B., and Hendrickson, W.A. (2015). Protein structure.Structure and activity of tryptophan-rich TSPO proteins. Science *347*, 551–555.

Hachez, C., Veljanovski, V., Reinhardt, H., Guillaumot, D., Vanhee, C., Chaumont, F., and Batoko, H. (2014). The Arabidopsis abiotic stress-induced TSPO-related protein reduces cellsurface expression of the aquaporin PIP2;7

through protein-protein interactions and autophagic degradation. Plant Cell *26*, 4974–4990.

Hammond, G.R., Fischer, M.J., Anderson, K.E., Holdich, J., Koteci, A., Balla, T., and Irvine, R.F. (2012). PI4P and PI(4,5)P2 are essential but independent lipid determinants of membrane identity. Science *337*, 727–730.

Heilmann, I. (2016). Phosphoinositide signaling in plant development. Development *143*, 20442055.

Hetherington, A.M., and Brownlee, C. (2004). The generation of Ca(2+) signals in plants. Annu. Rev. Plant Biol. *55*, 401–427.

Hirayama, T., Ohto, C., Mizoguchi, T., and Shinozaki, K. (1995). A gene encoding a phosphatidylinositol-specific phospholipase C is induced by dehydration and salt stress in Arabidopsis thaliana. Proc. Natl. Acad. Sci. U S A *92*, 3903–3907.

Holthuis, J.C., and Menon, A.K. (2014). Lipid landscapes and pipelines in membrane homeostasis. Nature *510*, 48–57.

Hong, S.H., Choi, H.B., Kim, S.U., and McLarnon, J.G. (2006). Mitochondrial ligand inhibits store-operated calcium influx and COX-2 production in human microglia. J. Neurosci. Res. *83*, 1293–1298.

Hong, Y., Zhao, J., Guo, L., Kim, S.C., Deng, X., Wang, G., Zhang, G., Li, M., and Wang, X. (2016). Plant phospholipases D and C and their diverse functions in stress responses. Prog. Lipid Res. *62*, 55–74.

Hunt, L., Mills, L.N., Pical, C., Leckie, C.P., Aitken, F.L., Kopka, J., Mueller-Roeber, B., McAinsh, M.R., Hetherington, A.M., and Gray, J.E. (2003). Phospholipase C is required for the control of stomatal aperture by ABA. Plant J. *34*, 47–55.

Im, Y.J., Perera, I.Y., Brglez, I., Davis, A.J., Stevenson-Paulik, J., Phillippy, B.Q., Johannes, E., Allen, N.S., and Boss, W.F. (2007). Increasing plasma membrane phosphatidylinositol(4,5) bisphosphate biosynthesis increases phosphoinositide metabolism in Nicotiana tabacum. Plant Cell *19*, 1603–1616.

Ischebeck, T., Stenzel, I., and Heilmann, I. (2008). Type B phosphatidylinositol-4-phosphate 5-kinases mediate Arabidopsis and Nicotiana tabacum pollen tube growth by regulating apical pectin secretion. Plant Cell *20*, 3312–3330.

Ischebeck, T., Stenzel, I., Hempel, F., Jin, X., Mosblech, A., and Heilmann, I. (2011). Phosphatidylinositol-4,5-bisphosphate influences Nt-Rac5-mediated cell expansion in pollen tubes of Nicotiana tabacum. Plant J. *65*, 453–468.

Jaremko, L., Jaremko, M., Giller, K., Becker, S., and Zweckstetter, M. (2014). Structure of the mitochondrial translocator protein in complex with a diagnostic ligand. Science *343*, 13631366.

Kooijman, E.E., Tieleman, D.P., Testerink, C., Munnik, T., Rijkers, D.T., Burger, K.N., and de Kruijff, B. (2007). An electrostatic/hydrogen bond switch as the basis for the specific interaction of phosphatidic acid with proteins. J. Biol. Chem. *282*, 11356–11364.

Kreps, J.A., Wu, Y., Chang, H.S., Zhu, T., Wang, X., and Harper, J.F. (2002). Transcriptome changes for Arabidopsis in response to salt, osmotic, and cold stress. Plant Physiol. *130*, 21292141.

Lavisse, S., Guillermier, M., Hérard, A.S., Petit, F., Delahaye, M., Van Camp, N., Ben Haim, L., Lebon, V., Remy, P., Dollé, F., et al. (2012). Reactive astrocytes overexpress TSPO and are detected by TSPO positron emission tomography imaging. J. Neurosci. *32*, 10809–10818.

Lee, Y., and Assmann, S.M. (1991). Diacylglycerols induce both ion pumping in patch-clamped guard-cell protoplasts and opening of intact stomata. Proc. Natl. Acad. Sci. U S A *88*, 2127–2131.

Lee, Y., Kim, Y.W., Jeon, B.W., Park, K.Y., Suh, S.J., Seo, J., Kwak, J.M., Martinoia, E., and Hwang, I. (2007). Phosphatidylinositol 4,5-bisphosphate is important for stomatal opening. Plant J. *52*, 803–816.

Li, F., Liu, J., Liu, N., Kuhn, L.A., Garavito, R.M., and Ferguson-Miller, S. (2016). Translocator protein 18 kDa (TSPO): an old protein with new functions? Biochemistry *55*, 2821–2831.

Li, F., Liu, J., Zheng, Y., Garavito, R.M., and Ferguson-Miller, S. (2015). Protein structure. Crystal structures of translocator protein (TSPO) and mutant mimic of a human polymorphism. Science *347*, 555–558.

Lin, R., Angelin, A., Da Settimo, F., Martini, C., Taliani, S., Zhu, S., and Wallace, D.C. (2014). Genetic analysis of dTSPO, an outer mitochondrial membrane protein, reveals its functions in apoptosis, longevity, and Ab42-induced neurodegeneration. Aging Cell *13*, 507–518.

Liu, K., Li, L., and Luan, S. (2005). An essential function of phosphatidylinositol phosphates in activation of plant shaker-type K+ channels. Plant J. *42*, 433–443.

Liu, L., Zhang, K., Sandoval, H., Yamamoto, S., Jaiswal, M., Sanz, E., Li, Z., Hui, J., Graham, B.H., Quintana, A., et al. (2015). Glial lipid droplets and ROS induced by mitochondrial defects promote neurodegeneration. Cell *160*, 177–190.

Ma, X., Shatil-Cohen, A., Ben-Dor, S., Wigoda, N., Perera, I.Y., Im, Y.J., Diminshtein, S., Yu, L., Boss, W.F., Moshelion, M., et al. (2015). Do phosphoinositides regulate membrane water permeability of tobacco protoplasts by enhancing the aquaporin pathway? Planta *241*, 741–755.

Marginedas-Freixa, I., Hattab, C., Bouyer, G., Halle, F., Chene, A., Lefevre, S.D., Cambot, M., Cueff, A., Schmitt, M., Gamain, B., et al. (2016). TSPO ligands stimulate ZnPPIX transport and ROS accumulation leading to the inhibition of P. falciparum growth in human blood. Sci. Rep. *6*, 33516.

Marsh, J.A., Singh, V.K., Jia, Z., and Forman-Kay, J.D. (2006). Sensitivity of secondary structure propensities to sequence differences between alpha- and gamma-synuclein: implications for fibrillation. Protein Sci. *15*, 2795–2804.

Mishra, G., Zhang, W., Deng, F., Zhao, J., and Wang, X. (2006). A bifurcating pathway directs abscisic acid effects on stomatal closure and opening in Arabidopsis. Science *312*, 264–266.

Morin, D., Musman, J., Pons, S., Berdeaux, A., and Ghaleb, B. (2016). Mitochondrial translocator protein (TSPO): from physiology to cardioprotection. Biochem. Pharmacol. *105*, 1–13.

Munnik, T., and Nielsen, E. (2011). Green light for polyphosphoinositide signals in plants. Curr. Opin. Plant Biol. *14*, 489–497.

Nakashima, A., Sato, T., and Tamanoi, F. (2010). Fission yeast TORC1 regulates phosphorylation of ribosomal S6 proteins in response to nutrients and its activity is inhibited by rapamycin. J. Cell Sci. *123*, 777–786.

Ozaki, H., Zoghbi, S.S., Hong, J., Verma, A., Pike, V.W., Innis, R.B., and Fujita, M. (2010). In vivo binding of protoporphyrin IX to rat translocator protein imaged with positron emission tomography. Synapse *64*, 649–653.

Papadopoulos, V., Baraldi, M., Guilarte, T.R., Knudsen, T.B., Lacapère, J.J., Lindemann, P., Norenberg, M.D., Nutt, D., Weizman, A., Zhang, M.R., et al. (2006). Translocator protein (18kDa): new nomenclature for the peripheral-type benzodiazepine receptor based on its structure and molecular function. Trends Pharmacol. Sci. *27*, 402–409.

Peters, C., Li, M., Narasimhan, R., Roth, M., Welti, R., and Wang, X. (2010). Nonspecific phospholipase C NPC4 promotes responses to abscisic acid and tolerance to hyperosmotic stress in Arabidopsis. Plant Cell *22*, 2642–2659.

Rupprecht, R., Papadopoulos, V., Rammes, G., Baghai, T.C., Fan, J., Akula, N., Groyer, G., Adams, D., and Schumacher, M. (2010). Translocator protein (18 kDa) (TSPO) as a therapeutic target for neurological and psychiatric disorders. Nat. Rev. Drug Discov. *9*, 971–988.

Sancak, Y., Bar-Peled, L., Zoncu, R., Markhard, A.L., Nada, S., and Sabatini, D.M. (2010). Ragulator-Rag complex targets mTORC1 to the lysosomal surface and is necessary for its activation by amino acids. Cell *141*, 290–303.

Sanchez, J.P., and Chua, N.H. (2001). Arabidopsis PLC1 is required for secondary responses to abscisic acid signals. Plant Cell *13*, 1143–1154.

Schroeder, J.I., Kwak, J.M., and Allen, G.J. (2001). Guard cell abscisic acid signalling and engineering drought hardiness in plants. Nature *410*, 327–330.

Seki, M., Narusaka, M., Ishida, J., Nanjo, T., Fujita, M., Oono, Y., Kamiya, A., Nakajima, M., Enju, A., Sakurai, T., et al. (2002). Monitoring the expression profiles of 7000 Arabidopsis genes under drought, cold and high-salinity stresses using a full-length cDNA microarray. Plant J. *31*, 279–292.

Simon, M.L., Platre, M.P., Assil, S., van Wijk, R., Chen, W.Y., Chory, J., Dreux, M., Munnik, T., and Jaillais, Y. (2014). A multi-colour/multi-affinity marker set to visualize phosphoinositide dynamics in Arabidopsis. Plant J. *77*, 322–337.

Takahara, T., and Maeda, T. (2013). Evolutionarily conserved regulation of TOR signalling. J. Biochem. *154*, 1–10.

Tan, X., Thapa, N., Choi, S., and Anderson, R.A. (2015). Emerging roles of PtdIns(4,5)P2-beyond the plasma membrane. J. Cell Sci. *128*, 4047–4056.

Tan, X., Thapa, N., Liao, Y., Choi, S., and Anderson, R.A. (2016). PtdIns(4,5)P2 signaling regulates ATG14 and autophagy. Proc. Natl. Acad. Sci. U S A *113*, 10896–10901.

Testerink, C., and Munnik, T. (2005). Phosphatidic acid: a multifunctional stress signaling lipid in plants. Trends Plant Sci. *10*, 368–375.

Thoreen, C.C., Kang, S.A., Chang, J.W., Liu, Q., Zhang, J., Gao, Y., Reichling, L.J., Sim, T., Sabatini, D.M., and Gray, N.S. (2009). An ATP-competitive mammalian target of rapamycin inhibitor reveals rapamycin-resistant functions of mTORC1. J. Biol. Chem. *284*, 8023–8032.

Vanhee, C., Guillon, S., Masquelier, D., Degand, H., Deleu, M., Morsomme, P., and Batoko, H. (2011a). A TSPO-related protein localizes to the early secretory pathway in Arabidopsis, but is targeted to mitochondria when expressed in yeast. J. Exp. Bot. *62*, 497–508.

Vanhee, C., Zapotoczny, G., Masquelier, D., Ghislain, M., and Batoko, H. (2011b). The Arabidopsis multistress regulator TSPO is a heme binding membrane protein and a potential scavenger of porphyrins via an autophagy-dependent degradation mechanism. Plant Cell *23*, 785–805.

Verma, A., Nye, J.S., and Snyder, S.H. (1987). Porphyrins are endogenous ligands for the mitochondrial (peripheral-type) benzodiazepine receptor. Proc. Natl. Acad. Sci. U S A *84*, 22562260.

Wang, P., Hawkins, T.J., Richardson, C., Cummins, I., Deeks, M.J., Sparkes, I., Hawes, C., and Hussey, P.J. (2014). The plant cytoskeleton, NET3C, and VAP27 mediate the link between the plasma membrane and endoplasmic reticulum. Curr. Biol. *24*, 1397–1405.

Wang, H., Ma, Q., Qi, Y., Dong, J., Du, X., Rae, J., Wang, J., Wu, W.F., Brown, A.J., Parton, R.G., et al. (2019). ORP2 delivers cholesterol to the plasma membrane in exchange for phosphatidylinositol 4, 5-bisphosphate (PI(4,5)P_2). Mol. Cell *73*, 458–473.e7.

Weisman, R., and Choder, M. (2001). The fission yeast TOR homolog, tor1+, is required for the response to starvation and other stresses via a conserved serine. J. Biol. Chem. *276*, 70277032.

Yakir-Tamang, L., and Gerst, J.E. (2009). A phosphatidylinositol-transfer protein and phosphatidylinositol-4-phosphate 5-kinase control Cdc42 to regulate the actin cytoskeleton and secretory pathway in yeast. Mol. Biol. Cell *20*, 3583–3597.

Yeliseev, A.A., and Kaplan, S. (1999). A novel mechanism for the regulation of photosynthesis gene expression by the TspO outer membrane protein of Rhodobacter sphaeroides 2.4.1. J. Biol. Chem. *274*, 21234–21243.

Yeliseev, A.A., Krueger, K.E., and Kaplan, S. (1997). A mammalian mitochondrial drug receptor functions as a bacterial "oxygen" sensor. Proc. Natl. Acad. Sci. U S A *94*, 5101–5106.

Yen, H.Y., Hoi, K.K., Liko, I., Hedger, G., Horrell, M.R., Song, W., Wu, D., Heine, P., Warne, T., Lee, Y., et al. (2018). PtdIns(4,5)P. Nature *559*, 423–427.

Zheng, L., Shan, J., Krishnamoorthi, R., and Wang, X. (2002). Activation of plant phospholipase Dbeta by phosphatidylinositol 4,5-bisphosphate: characterization of binding site and mode of action. Biochemistry *41*, 4546–4553.

Zimmermann, P., Hirsch-Hoffmann, M., Hennig, L., and Gruissem, W. (2004). GENEVESTIGATOR.Arabidopsis microarray database and analysis toolbox. Plant Physiol. *136*, 2621–2632.

iScience, Volume *23*

Supplemental Information

A Plant-Specific N-terminal Extension Reveals Evolutionary Functional Divergence within Translocator Proteins

Pawel Jurkiewicz, Lucile Senicourt, Haitham Ayeb, Olivier Lequin, Jean-Jacques Lacapere, and Henri Batoko

TRANSPARENT METHODS

Plant material

We used *A. thaliana* (ecotype Columbia-0) WT and transgenic plants expressing full-length AtTSPO, point-mutated AtTSPO^{H91A} or Venus-tagged AtTSPO$^{\Delta N}$ (first 41 amino acids removed), all under the control of the p35S promoter (Guillaumot et al., 2009; Vanhee et al., 2011b). An Arabidopsis homozygous T-DNA insertional line (KO) in TSPO (Guillaumot et al., 2009) was also used. Seed origin, sterilisation and growth conditions were as described previously (Guillaumot et al., 2009; Vanhee et al., 2011).

To generate the AtTSPO overexpressing cassette, AtTSPO cDNA (RIKEN, clones RAFL09-68-G14 and RAFL05-18-I12) was PCR-amplified and the PCR product was digested with XbaI/BglII and cloned into pPily (Ferrando et al., 2000) opened with XbaI/BamHI to generate pPily-AtTSPO. The expression cassette driven by a double p35S promoter in pPily was retrieved by digestion with Acc65I and subcloned into pCAMBIA 1300 opened with the same enzyme. To generate the AtTSPO^{H91A} overexpressing cassette, the cDNA of AtTSPO variant H91A was cloned from p426GAL1-AtTSPO^{H91A} (Vanhee et al., 2011b), digested with XbaI/BglII and cloned into pPILY digested with the same restriction enzymes. The expression cassette containing a double p35S promoter was retrieved from pPILY using NotI and subcloned into pAUX-3131 opened with NotI, then into the binary vector pMODUL using I-SCEI (Goderis et al., 2002). The generation of Venus-AtTSPOdeltaN was as for the AtTSPO overexpressing cassette described above except that the first 41 residues of AtTSPO were replaced by the fluorescent protein Venus sequence. The KO plants were offspring of Arabidopsis homozygous T-DNA insertional line in *TSPO* (SALK_066561C). All plasmids were amplified in *Escherichia coli* DH5α and the plasmid was transferred into *Agrobacterium tumefaciens* GV3101 containing the Ti plasmid pMP90 (a gift from Dr C. Koncz, MPI, Cologne, Germany) for Arabidopsis transformation.

Transgenic *A. thaliana* Columbia-0 plants were generated by the standard floral dip method (Clough and Bent, 1998). To this end, plants were grown until flowering and all the fertilized siliques were removed before dipping. *A. tumefaciens* GV3101 bacteria grown in a liquid medium supplemented with appropriate antibiotics were harvested in the mid-log phase. The culture was spun down and resuspended in 5% sucrose solution followed by addition of 0.02% Silwet L-77 surfactant (Lehle Seeds, Round Rock, USA, #VIS-01). The above-ground parts of plants were dipped in bacterial solution for 2-3 seconds with gentle agitation. Then, the pots

with plants were laid on their side, covered by plastic foil to maintain high humidity and put back in a room under dimmed light.

Twenty-four hours later, plants were transferred into the phytotron and further grown under normal watering regime (twice a week) until seeds became mature. Seeds were harvested and screened for homozygous transformants using 20 µg/ml hygromycin B.

Seeds spread on a filter paper were disinfected under laminar flow hood first by pouring 70% ethanol containing 0.02% Silwet L-77 surfactant followed by 3 rounds with 100% ethanol. After each round, the seeds were allowed to dry and after the sterilization process they were brushed off on the agar plate containing appropriate medium. Seeds were stratified for 2–3 days at 4°C in the dark, and transferred into a growth chamber (16h/8h light/dark regime, 22–25°C, 90 µmol photons. $s^{-1}.m^{-2}$). After germination and growth for 10 days on the agar plate, the seedlings were transferred to Jiffy pots (http://www.jiffypot.com) for further growth in soil or subjected to various treatments.

WT Arabidopsis suspension cells (May and Leaver, 1993) were agitated in the dark on a rotary shaker and diluted 10-fold weekly in freshly sterilised LS medium (Duchefa, Haarlem, The Nederlands, #L0230; 4.43 g/L) adjusted to pH 5.7 with KOH and containing 3% sucrose, 50 µg/L kinetin (Duchefa # K0905), and 500 µg/L 1-naphthalene acetic acid (Duchefa #N0903).

Water loss and stomatal conductance assays

To assess dehydration tolerance, WT, TSPO knockout, AtTSPO, $AtTSPO^{H91A}$ and Venus-$AtTSPO^{\Delta N}$ overexpressing plants were grown on half-strength Murashige and Skoog (MS) agar plates (0.2% MS basal salt mixture, MP Biomedicals, Eschewege, Germany, #0926230) containing 1% sucrose, 25 mM 2-(N-morpholine)-ethanesulphonic acid (MES, Sigma-Aldrich, Overijse, Belgium, #69889), pH 5.7, sealed with parafilm in a growth chamber (16 h/8 h light/dark, 22-25°C, 90 µmol photons.s^{-1} .m^{-2}). The 7-day-old seedlings were transferred from agar plates into pots with soil, installed in the phytotron (16 h/8 h light/dark, 20°C, 65% humidity, 120 µmol photons.s^{-1} .m^{-2}) and watered twice weekly. Integral rosette leaves of pre-flowering plants were subjected to abaxial stomatal conductance measurements according to the manufacturer's protocol (automatic mode, SC-1 Leaf Porometer; Decagon Devices, Pullman, USA).

To assess the water loss on detached rossette leaves, the seeds of wild-type, TSPO knockout and AtTSPO, $AtTSPO^{H91A}$ and Venus-$AtTSPO^{\Delta N}$ overexpressing plants were put on soil in a phytotron (average temperature 20°C, approx. 65% humidity, 16 h photoperiod,

~120 µmol.m^{-2}.s^{-1}). Seventeen days after germination, rosettes were isolated using a blade and then were transferred on a weighing paper and weighted on a microbalance at time 0 and after 120 minutes. Water loss was expressed as percentage of the original weight of seedlings. For this experiment, we assayed five rosettes of each genotype harvested from at least two pots (pots were randomly allocated in different areas of phytotron).

Transformation of plant suspension cells and PM preparation

Transgenic Arabidopsis suspension cell lines were co-cultivated with Agrobacterium (Van Leene et al., 2007) (Timentin, Duchefa #T-104-2, replaced vancomycin). The pCambia3300 USER vector cloning system (Nour-Eldin et al., 2006) was used to generate mGFP5-TSPO fusions driven by the p35S promoter. GFP-tagged AtTSPO, AtTSPO$^{\Delta N}$, mTSPO (mouse homolog) and AtTSPO^{Nter}-mTSPO (N-terminus of AtTSPO added to the mouse protein) chimeras were created by PCR using primers listed in Supplemental Table S1. For GFP-AtTSPO$^{\Delta N}$, a seven amino acid linker (GAGAGAG) was introduced to increase flexibility of the chimeric protein.

The vector harboring the PI(4,5)P_2 phosphoinositide sensor (Simon et al., 2014) was a generous gift from Dr Yvon Jaillais (Ecole Normale Supérieure, Lyon, France) and Dr Teun Munnik (University of Amsterdam, The Netherlands).

Plasma membrane-enriched fractions of WT and transgenic Arabidopsis suspension cells were prepared by two-phase partitioning of microsomal fraction (Santoni et al., 2006). All the steps were performed at 4°C. To obtain microsomal membranes, cells were harvested and mechanically disrupted by glass beads in a disruption buffer (2.5 mL buffer/g fresh cells; 50 mM Tris pH 8, 500 mM sucrose, 10% glycerol, 20 mM EDTA, 20 mM EGTA, 50 mM NaF, 10 mM ascorbic acid, 0.6% w/v polyvinylpyrrolidone, 5 mM dithiothreitol and protease inhibitors). The cell homogenate was centrifuged at 10000 g for 10 min and the supernatant was filtered through a 100 µm-diameter nylon cloth. Finally, microsomal pellet was obtained from the supernatant by centrifugation at 50000 g for 35 min.

Nine grams of microsomal fraction was mixed with 27 g of phase system (11.82 g Dextran T-500 20% w/w (Sigma #31392), 5.76 g polyethylene glycol 3350 40% w/w (Sigma #P4338), 5 mM phosphate buffer pH 7.8, 5 mM KCl, 300 mM sucrose, H2O up to 27 g). The mixture was shaken vigorously 15-20 times and allowed to separate out into two phases by centrifugation at 2000 g for 10 min. To purify the PM from the upper phase, this phase was repartitioned against a “fresh” lower phase. “Fresh” lower phase was obtained after centrifugation of a shaken

mixture of 9 g of microsomal buffer and 27 g of phase system. After a series of fractions' repartitioning, the PM-containing phases were diluted in 60 mL of PM washing buffer (10 mM Tris pH 8.3, 10 mM boric acid, 300 mM sucrose, 9 mM KCl, 5 mM EDTA, 5 mM EGTA, 50 mM NaF, 5 mM dithiothreitol, protease inhibitors) before pelleting for 35 min at 85 000g max. Pelleted PM-enriched fraction was resuspended in PM washing buffer, frozen in liquid nitrogen and stored for a short term (days) at -20°C or for a long term (weeks) at -80°C.

BiFC experiments and cell imaging

For BiFC assays, we employed the pDOE12 vector (Gookin and Assmann, 2014) (provided by Dr Sarah Assmann, Pennsylvania State University, USA) encoding a split Venus at the N-terminus of the protein of interest (Venus split into 210 and 29 amino acid N and C parts, respectively). Full-length AtTSPO and AtPIP2;7 cDNAs were PCR-amplified from templates (Vanhee et al., 2011a; Hachez et al., 2014), and N-terminally truncated variants of AtTSPO were generated by PCR. All AtTSPO lysine/arginine point mutants were created by overlapping PCR-mediated site-directed mutagenesis using primers listed in Supplemental Table S1. Transient expression in tobacco (*Nicotiana tabacum*) was performed using *Agrobacterium tumefaciens*-mediated transfection as described previously (Batoko et al. 2000). *N. tabacum* Petit Havana seeds were put on soil and grown at 21°C until the seedling stage (but no flowers) has well established. Each expression vector was introduced by electroporation into *A. tumefaciens* GV3101 (pMP90) strain (Koncz and Schell, 1986). A single colony from the transformants was used to inoculate 2 mL of YEB medium (w/v: 0.5% beef extract, 0.1% yeast extract, 0.5% sucrose, and 2 mM $MgSO_4$), supplemented with 100 mg/mL kanamycin and 20 mg/mL gentamycin. On the next day, 1 ml of culture was transferred into an Eppendorf tube, and the bacteria were pelleted by centrifugation at 2200 g for 5 min at room temperature. The pellet was washed twice with 1 mL of the infiltration buffer (10 mM MES pH 5.6-5.7, 0.5% glucose (w/v), 20 mM $MgSO_4$ and 100 µM acetosyringone (Sigma, Overijse, Belgium)) and then resuspended in 1 mL of the same buffer.

The bacterial suspension was diluted with infiltration buffer to adjust the inoculum concentration to the OD_{600} value of 0.2. The inoculum was delivered to the lamina tissues of tobacco leaves by gentle pressure infiltration through the stomata of the lower epidermis, by using a 1 ml syringe without a needle. The infected area of the leaf was delimited and labeled with an indelible pen, and the plant was incubated under normal growing conditions as above. One tobacco plant was used to infiltrate one genetic construct.

Confocal imaging with a Zeiss LSM710 confocal microscope equipped with a spectral detector was performed as described (Guillaumot et al., 2009; Vanhee et al., 2011a; Hachez et al., 2014). Reconstituted mVenus fluorescence after BiFC was excited with a 514 nm argon multiline laser and the amplified emitted light was recorded between 520 and 610 nm. mTurquoise was excited with a 445 nm laser, and fluorescence used to detect transfected cells and Golgi colocalisation of the BiFC signal. Images were processed using identical parameters. To quantify the BiFC signal, we imaged five randomly chosen independent (non-overlapping) areas of infiltrated or non-infiltrated leaves. Pixel intensities from mTurquoise and mVenus channels were acquired along two diagonals of each image (~700 intensity measurements per diagonal) using ZEN2012 software (Carl Zeiss, Oberkochen, Germany). Average signal intensities were calculated from 10 diagonals, and values for non-infiltrated leaves were subtracted. Ratios between the BiFC/mTurquoise signal intensities were calculated and normalised against full-length AtPIP2;7-AtTSPO positive control.

Human phosphatidylinositol 4-phosphate 5-kinase type-1 (PI4P 5-kinase) alpha fused to mCherry (mCherry-HsPIPK1α) known to be functional in plant cells (Ma et al., 2015) was expressed in tobacco leaves by Agrobacterium-mediated transient expression. The construct was expressed in WT plants and stable transgenic lines overexpressing YFP-AtTSPO. Confocal imaging of the resulting mCherry signal in leaf epidermal cells was performed using a 561 nm 543 excitation laser.

TSPO purification for *in vitro* biochemical assays

Yeast transformation was performed by the LiAc/ss-DNA/PEG method as described (Gietz and Schiestl, 2007). A freshly grown colony of yeast on a solid plate was suspended in 1 ml of sterile miliQ water. Cells were vortexed and then centrifuged at 13000 g for 30 s. The supernatant was discarded and the yeast pellet was covered (the order as given) with 240 µl PEG 3350 (50% w/v), 36 µl lithium acetate (1 M), 50 µl single-stranded DNA (2 mg/ml, to obtain a single-stranded state, the DNA from fish sperm was boiled 5 min followed by a snap cool on ice), and finally 34 µl of sterile water and approximately 25-50 ng of plasmid DNA of interest. The content of the tube was vortexed until resuspended. Then, the tube was placed in a water bath at 42°C and incubated for 20 min. After this period, cells were pelleted at 13000 g for 30 s at room temperature and the transformation mix supernatant was removed. Cells were resuspended gently in 1 ml of sterile water and plated (100 µl and 900 µl) on a selective medium. Colonies of transformants were screened for the presence of gene of interest by colony PCR.

Ten histidine-tagged AtTSPO and AtTSPO$^{\Delta N}$ proteins were expressed and purified from microsomal membranes of *Saccharomyces cerevisiae* (Vanhee et al., 2011b). Microsomes were suspended in solubilization buffer (50 mM Tris pH 8, 500 mM NaCl, 10% glycerol, 20 mM imidazole, protease inhibitors) and solubilized with 2% n-Dodecyl β-D-maltoside (DDM, Enzo #ALX-500-007) for 30 min at room temperature. The mixture was centrifuged for 30 min at 20000 g at room temperature and solubilized proteins (in supernatant) were subsequently mixed with Ni-NTA matrix (Qiagen, Benelux, #30210) pre-equilibrated with solubilisation buffer lacking imidazole. Binding was performed at room temperature for 3 h, after which the flow-through was collected and beads were washed four times with wasing buffer (solubilization buffer containing 0.2% DDM) with increasing imidazole concentrations (20, 20, 40 and 60 mM). Bound proteins were eluted with 300 mM imidazole in washing buffer.

The 6His-mTSPO (pET-15b vector) and 10His-tagged AtTSPO N-terminus fused to mTSPO (AtTSPO^{Nter}-mTSPO; GST fusion in a pGEX-4T-2 vector) were expressed and purified from *Escherichia coli* BL21 (DE3). Protein expression was induced with 1 mM isopropyl-β-D-thiogalactoside (IPTG) at 28°C for 4 h, cells were centrifuged, and the pellet was resuspended in buffer A (50 mM TRIS pH 8.0, 300 mM NaCl, 10% glycerol, 20 mM imidazole) containing protease inhibitor cocktail (Sigma) supplemented with both 1 mg/ml lysozyme and 1000 U benzonase (Sigma-Aldrich, Overijse, Belgium, # E1014) and incubated for 15 min at room temperature with gentle shaking.

Cells were lysed by sonication (3 min, amplitude 60%, 10 s pulses; ultrasonic processor Vibra-Cell, Sonics & Materials, Newtown CT, USA). Bacterial membranes containing overexpressed TSPO were obtained after two centrifugation steps at 4°C by centrifuging lysed cells for 30 min at 15,000 g followed by supernatant centrifugation for 1 h at 250,000 g. Sedimented membranes were resuspended in buffer A and solubilised by adding n-dodecyl-β-D-maltoside (DDM; Enzo Life Sciences, Brussels, Belgium, #ALX-500-007) to a final concentration of 2% for 1 h at room temperature on a rotary wheel. Solubilised membranes were centrifuged at 150,000 g for 30 min at 4°C and the supernatant was mixed with Ni-NTA matrix (Qiagen, Benelux, #30210) pre-equilibrated with solubilisation buffer lacking imidazole. Purification was performed as described above. Bound proteins were eluted with 300 mM imidazole in buffer A and dialysed on PD-10 desalting columns (GE Healthcare, Belgium-Luxemburg, #17085101) against imidazole-free buffer A. Eluted fractions of mTSPO were pooled, concentrated and frozen in aliquots.

After dialysis, AtTSPO^{Nter}-mTSPO fusion proteins were subjected to a second purification step by overnight digestion at room temperature with His-tagged tobacco etch virus (TEV) protease (0.1 µg/ml; produced and provided by Marc Boutry's laboratory, UCLouvain, Louvain-la-Neuve, Belgium). The mixture was added to a nickel affinity column and processed as previously described. Washed fractions containing the protein of interest were pooled, dialysed, concentrated and frozen for subsequent biochemical analysis. Primers used for expression and purification of TSPO are listed in Supplemental Table S1.

Expression and purification of the N-terminus of AtTSPO for structural studies

The AtTSPO^{Nter} construct (residues 1-49) was expressed via pGEX-4T-2 vectors in *E. coli* BL21 (DE3) as a GST-fused 10His-tagged protein containing a TEV protease cleavage site. To obtain labelled protein, bacteria were cultured in M9 minimal medium supplemented with [^{15}N]-NH_4Cl and [^{13}C]-glucose at 1 and 4 g/L, respectively. Protein expression in cells cultured in the presence of 0.1 mg/ml ampicillin was induced with IPTG at 37°C for 4 h. Bacteria were collected and protease inhibitor cocktail was added before lysis (by sonication) in 50 mM HEPES-NaOH and 500 mM NaCl (pH 7.8), followed by centrifugation at 14,000 g for 20 min. Protein in the supernatant was purified using Ni-NTA resin and eluted with 250 mM imidazole. Purified proteins were dialysed against 50 mM HEPES-NaOH at pH 7.8 overnight at room temperature and then digested by His-tagged-TEV protease (0.1 µg/ml) overnight (16-20 h) at room temperature. Cleaved AtTSPO^{Nter} was isolated from GST-fusion proteins and proteases using Ni-NTA resin since His-tagged GST and TEV proteins were retained on the column.
Purified proteins were dialysed against 10 mM sodium phosphate and 1 mM NaN_3 at pH 7.8 to perform structural studies. SDS-PAGE analysis was performed on samples collected during all purification steps.
Purified AtTSPO^{Nter} was characterised by (i) dot blots and (ii) mass spectrometry (MS). For dot blots, spots of AtTSPO^{Nter} on PVDF membranes were first incubated with polyclonal rabbit anti-AtTSPO antibody serum followed by anti-rabbit antibody coupled to alkaline phosphatase, and visualisation with specific substrates (BCIP/NBT Sigma-Fast; Sigma-Aldrich, Overijse, Belgium, #B5655). For MS, aliquots of purified AtTSPO^{Nter} were mixed with HCCA matrix and analysed using a 5-17 kDa standard set protein (Proteomics Sigma-Aldrich, Overijse, Belgium) via MALDI-TOF (DE-Pro, ABSciex, Framingham, MA, USA). The concentration of purified AtTSPO^{Nter} was determined by UV spectroscopy in conjunction with the calculated

extinction coefficient (280 nm) of 0.256 for 1 mg/ml. Primers used for expression and purification of AtTSPO^{Nter} are listed in Supplemental Table S1.

Circular dichroism (CD) spectroscopy

CD measurements were carried out on a JASCO spectropolarimeter (JASCO, France) with a 1 mm cuvette at room temperature.

Preparation of bicelles and PI(4,5)P_2 micelles

Bicelles were prepared as previously described (Caillon et al., 2013). Briefly, 25 mM 1,2-dimyristoyl-sn-glycero-3-phosphocholine or 1,2-dimyristoyl-sn-glycero-3-phospho-(1'-*rac*-glycerol), corresponding to DMPC or DMPG, respectively (Avanti polar lipids) and 50 mM 1,2-dihexanoyl-sn-glycero-3-phosphocholine (DHPC; Avanti polar lipids) in 10 mM sodium phosphate at pH 6.1-6.2 were mixed (vortexed for 1 min) and subjected to three freeze-thaw cycles. Next, 1,2-dioleoyl-sn-glycero-3-phospho-(1'-myo-inositol-4',5'-bisphosphate) PI(4,5)P_2 micelles were formed by adding 10 mM sodium phosphate at pH 6.1-6.2 to powder and sonicating to ensure thorough mixing (stock solution 5 mM)

Dynamic light scattering (DLS)

LS measurements were carried out with a DynaPro-99 instrument (Yatt 616 Technology). The sizes (radius) of bicelles (DMPC/DMPG) and PI(4,5)P_2 micelles were determined to be 4.1±0.2 and 65±20 nm, respectively.

NMR spectroscopy

NMR samples were prepared in 5 mm NMR tubes and contained ~100 µM ^{15}N- and ^{13}C-labelled AtTSPO^{Nter} in 10 mM sodium phosphate at pH 6.2 and H2O/D2O (90:10 v/v). A 0.1 mM sample of sodium 2,2-dimethyl-2-silapentane-d6-5-sulfonate (DSS, Sigma) served as an internal chemical shift reference. Protease inhibitor cocktail (Roche) and EDTA (1 mM) were added to prevent degradation. Experiments were recorded on a Bruker 500 MHz Avance III spectrometer equipped with a TCI cryoprobe. Resonances were assigned using 2D ^{1}H-^{15}N HSQC and 3D ^{1}H-^{15}N-^{13}C HNCACB, CBCA(CO)NH, HNCA, HNCO and HN(CA)CO spectra acquired at 20°C. NMR data were processed with Bruker TopSpin 3.2 or NMRPipe and analysed with NMRFAM-SPARKY (Caillon et al., 2013; Delaglio et al., 1995; Lee et al., 2015; Ziarek et al., 2011).

Secondary structure analysis was based on SSP scores (Marsh et al., 2006) calculated from $^{13}C\alpha$, $^{13}C\beta$, ^{13}CO, ^{1}HN and ^{15}N chemical shifts.

Subsequent 2D ^{1}H-^{15}N-HSQC spectra of AtTSPO^{Nter} were recorded in the presence of DMPC/DHPC and DMPG/DHPC bicelles (12.5/25 mM, respectively; q = 0.5), and in the presence of increasing amounts of PI(4,5)P_2 at 1 to 10 equivalents. Both ^{1}H and ^{15}N chemical shift perturbations (CSP) were calculated using the following formula:

$\Delta\delta = \left| \Delta\delta(1H) \right| + 1/10 \left| \Delta\delta(15N) \right|$

where the binding constant (Kd) was estimated from CSP values upon titration with PI(4,5)P_2 using a fast-exchange single-site binding model (Delaglio et al., 1995).

Western blot and antibodies

Extracted proteins were quantified by the Bradford method, mixed with 5× Laemmli buffer and incubated for 30 min at 37°C prior to SDS-PAGE and transfer onto PVDF membranes (Immobilon-P, Merck-Millipore, Darmstadt, Germany, #IPVH00010) using the semi-dry transfer method. Membranes were saturated for 1 h at 25°C in blocking buffer (5% non-fat milk in TBS-Tween-20 supplemented with 0.5% Tween-20 in 1× TBS) and incubated at room temperature for 1 h with primary antibodies diluted in washing buffer (0.5% milk in TBS Tween-20 supplemented with 0.1% Tween-20 in 1× TBS). After washing three times in washing buffer, membranes were incubated with secondary Horseradish peroxidase (HRP)-conjugated antibodies for 1 h at room temperature. After washing three times in washing buffer, membranes were incubated for 3-5 min with ECL (Roche, #11500694001). Emitted light was detected using either a film processor (Optimax X-ray film processor; Protec Medical Systems) or a digital imaging device (Amersham Imager 600, GE Healthcare Life Sciences). All original immunoblots are provided as Supplemental Information.

Polyclonal anti-AtTSPO antibodies were designed by the host laboratory and raised in a rabbit against the synthetic peptide ^{2}DSQDIRYRGGDDRDA^{16} followed by affinity purification using the same peptide (Eurogentec) (Guillaumot et al., 2009).

HisProbe-HRP conjugates were purchased from ThermoFisher Scientific (#15165). Antibodies against Arabidopsis RbcL and AtPIP2;7 were purchased from Agrisera (#AS03037 and #AS09469, respectively). Anti-GFP was from Abcam (#ab290), and anti-PI(4,5)P_2 was from Enzo Life Sciences (#ADI-915-052-020). The mouse monoclonal anti-actin (β-actin) was purchased from Proteintech (#60008-1-Ig). Anti-FLAG was a generous gift from Dr Michel

Ghislain (UCLouvain, Louvain-la-Neuve, Belgium), and antibodies against plant H^+-ATPases were provided by Dr Marc Boutry (UCLouvain, Louvain-la-Neuve, Belgium).

For western blotting, anti-AtTSPO, anti-AtPIP2;7, anti-GFP and anti-RbcL antibodies were diluted 1:5,000, HisProbe-HRP was diluted 1:1,000, anti-PI(4,5)P_2 and anti-FLAG were diluted 1:2,000, and anti-H^+-ATPase was diluted 1:100,000. HRP-conjugated anti-rabbit and anti-mouse secondary antibodies were from Sigma and diluted 1:10,000.

Overlay and pull-down assays

Protein-lipid overlay assays were performed using commercially available PIP Strips (Echelon Biosciences, Salt Lake City, USA, #P-6001) according to manufacturer's protocols, or using membranes prepared in our laboratory. Briefly, phosphatidic acid (Sigma-Aldrich, Overijse, Belgium, #P9511, dissolved in $CHCl_3$), phosphoinositides PI3P, PI4P and PI(4,5)P_2 (Echelon Biosciences, #P-3016, #P-4016 and #P-4516, respectively; all dissolved in 2% DDM), or SDS-solubilised plasma membrane fractions were spotted on nitrocellulose membranes (Amersham Protran, GE Healthcare, #10600002) and air dried for 1 h. Membranes were then saturated in blocking buffer (3% BSA in TBS-Tween-20, supplemented with 0.1% Tween-20 in TBS). Incubation with proteins in blocking buffer was performed at room temperature for 3 h, followed by incubation with primary and secondary antibodies and ECL exposure as described above.

For lipid-dependent pull-down assays, purified 10His-AtTSPO or 10His-AtTSPO$^{\Delta N}$ were incubated for 3 h at room temperature with phosphatidic acid-coupled agarose beads (Echelon Biosciences, #P-B0PA) followed by flow-through collection, three washes with incubation buffer (50 mM TRIS-HCl pH 8.0, 150 mM NaCl, 10% glycerol, 0.2% DDM, proteases inhibitors) and elution with Laemmli buffer supplemented with 8 M urea. Uncoupled agarose beads were used as a negative control.

Microscale thermophoresis (MST)

MST was used to investigate binding events between purified TSPO and lipid or aquaporin ligands. All experiments were performed on a Monolith NT115 instrument (Nanotemper Technologies, Germany) equipped with red and green filters using standard treated capillaries. Proteins and lipids were stored in the same buffer composed of 50 mM TRIS-HCl pH 8.0, 200 mM NaCl, 10% glycerol, 2% DDM, and proteases inhibitors (Sigma-Aldrich, Overijse, Belgium). Proteins were titrated against a gradient of lipid concentrations, and in the PIP2;7-

AtTSPO interaction assay, PIP2;7 was titrated against different AtTSPO concentrations. In the phosphatidic acid binding experiment, full-length AtTSPO and isolated N-termini were labelled on lysine residues with NT-647-NHS, while PI(4,5)P_2 binding assay proteins were labelled on polyhistidine tags with RED-tris-NTA (Nanotemper, Müchen, Germany). YFP-AtPIP2;7 aquaporin (mVenus variant) was in the form of a DDM-solubilised microsomal fraction of transgenic *A. thaliana* seedlings (Hachez et al., 2014), and YFP fluorescence was probed using a green filter. The laser power was set to 10, 20 or 40%, and the LED power was maintained at 100%.

PLC activity assay

We used the EnzCheck® Direct Phospholipase C Assay kit to measure PLC activity from plant extract according to the manufacturer recommendations. We used the PC-PLC from *Bacillus cereus* present in the kit to normalize the recorded fluorescence emission. Plant extract were obtained from 10-day-old Arabidopsis seedlings growing on MS plate. For ABA treatment, the seedling were incubated for 24 hours in half-strength MS containing 50 µM ABA and in the dark. PLC activity was measured in triplicate (total protein per reaction: 10 µg, 30 µg and 90 µg) and the experiment repeated at least twice.

Statistical analysis

The number of replicates and statistical methods for each experiment are stated within figure legends. GraphPad Prism version 5.03 for Windows (GraphPad Software; San Diego, California, USA; www.graphpad.com) was used to analyse statistical significance. For western blot signal quantification, we used ImageJ version 1.51j8 (NIH, USA; www.imagej.nih.gov/ij/). For quantification, we ensured that exposure conditions provided by the digital imager were below the saturation threshold. For MST data analysis, we used NT Analysis 1.5.37 software (Nanotemper, Müchen, Germany). A non-linear regression model was used (Graphpad Prism) to fit normalised fluorescence data and derive binding constants.

Supplemental references:

Batoko, H., Zheng, H.Q., Hawes, C., and Moore, I. (2000). A rab1 GTPase is required for transport between the endoplasmic reticulum and golgi apparatus and for normal golgi movement in plants. Plant Cell 12, 2201-2218.

Caillon, L., Lequin, O., and Khemtémourian, L. (2013). Evaluation of membrane models and their composition for islet amyloid polypeptide-membrane aggregation. Biochim Biophys Acta 1828, 2091-2098.

Clough, S.J., and Bent, A.F. (1998). Floral dip: a simplified method for Agrobacteriummediated transformation of Arabidopsis thaliana. Plant J 16, 735-743.

Delaglio, F., Grzesiek, S., Vuister, G.W., Zhu, G., Pfeifer, J., and Bax, A. (1995). NMRPipe: a multidimensional spectral processing system based on UNIX pipes. J Biomol NMR 6, 277-293.

Ferrando, A., Farras, R., Jasik, J. and Schell, J. (2000). Intron-tagged epitope: a tool for facile detection and purification of proteins expressed in Agrobacterium-transformed plant cells. Plant J 22, 553-560.

Gietz, R.D. and Schiestl, R.H. (2007). High-effiency yeast transformation using the LiAc/SS carrier DNA/PEG method. Nat Protoc 2, 31-34.

Goderis, I.J. W.M., De Bolle, M.F.C., François, I.E.J.A., Wouters, P.F.J, Broekaert, W.F., and Cammue, B.P.A. (2002). A set of modular plant transformation vectors allowing flexible insertion of up to six expression units. Plant Mol Biol 50, 17-27.

Guillaumot, D., Guillon, S., Déplanque, T., Vanhee, C., Gumy, C., Masquelier, D., Morsomme, P., and Batoko, H. (2009). The Arabidopsis TSPO-related protein is a stress and abscisic acidregulated, endoplasmic reticulum-Golgi-localized membrane protein. Plant J 60, 242-256.

Hachez, C., Veljanovski, V., Reinhardt, H., Guillaumot, D., Vanhee, C., Chaumont, F., and Batoko, H. (2014). The Arabidopsis abiotic stress-induced TSPO-related protein reduces cell surface expression of the aquaporin PIP2;7 through protein-protein interactions and autophagic degradation. Plant Cell 26, 4974-4990.

Koncz, C. and Schell, J. (1986). The promoter of TL-DNA gene 5 controls the tissue-specific expression of chimaeric genes carried by a novel type of Agrobacterium binary vector. MGG 204, 386-396.

Lee, W., Tonelli, M., and Markley, J.L. (2015). NMRFAM-SPARKY: enhanced software for biomolecular NMR spectroscopy. Bioinformatics 31, 1325-1327.

Ma, X., Shatil-Cohen, A., Ben-Dor, S., Wigoda, N., Perera, I.Y., Im, Y.J., Diminshtein, S., Yu, L., Boss, W.F., Moshelion, M., et al. (2015). Do phosphoinositides regulate membrane water permeability of tobacco protoplasts by enhancing the aquaporin pathway? Planta 241, 741-755.

Marsh, J.A., Singh, V.K., Jia, Z., and Forman-Kay, J.D. (2006). Sensitivity of secondary structure propensities to sequence differences between α- and γ-synuclein: Implications for fibrillation. Protein Sci 15, 2795-2804.

May, M.J., and Leaver, C.J. (1993). Oxidative Stimulation of Glutathione Synthesis in Arabidopsis thaliana Suspension Cultures. Plant Physiol 103, 621-627.

Nour-Eldin, H.H., Hansen, B.G., Nørholm, M.H., Jensen, J.K., and Halkier, B.A. (2006). Advancing uracil-excision based cloning towards an ideal technique for cloning PCR fragments. Nucleic Acids Res 34, e122.

Santoni, V., Verdoucq, L., Sommerer, N., Vinh, J., Pflieger, D., and Maurel, C. (2006).

Methylation of aquaporins in plant plasma membrane. Biochem J 400, 189-197.

Simon, M.L., Platre, M.P., Assil, S., van Wijk, R., Chen, W.Y., Chory, J., Dreux, M., Munnik, T., and Jaillais, Y. (2014). A multi-colour/multi-affinity marker set to visualize phosphoinositide dynamics in Arabidopsis. Plant J 77, 322-337.

Vanhee, C., Guillon, S., Masquelier, D., Degand, H., Deleu, M., Morsomme, P., and Batoko, H. (2011a). A TSPO-related protein localizes to the early secretory pathway in Arabidopsis, but is targeted to mitochondria when expressed in yeast. J Exp Bot 62, 497-508.

Vanhee, C., Zapotoczny, G., Masquelier, D., Ghislain, M., and Batoko, H. (2011b). The Arabidopsis multistress regulator TSPO is a heme binding membrane protein and a potential scavenger of porphyrins via an autophagy-dependent degradation mechanism. Plant Cell 23, 785-805.

Van Leene, J., Stals, H., Eeckhout, J., Persiau, G., Van De Slijke, E., Van Isterdael, G., De Clercq, A., Bonnet, E., Laukens, K., Remmerie, N, Henderickx, K, De Vijlder, T., Abdelkrim, A., Pharazyn, A., Van Onckelen, H., Inzé, D., Witter, E., and De Jaeger, G. (2007). A tandem affinity purification-based technology platform to study the cell cycle interactome in Arabidopsis thaliana. Mol Cell Prot 6, 1226-1238.

Ziarek, J.J., Peterson, F.C., Lytle, B.L., and Volkman, B.F. (2011). Binding site identification and structure determination of protein-ligand complexes by NMR a semiautomated approach.

Methods Enzymol 493, 241-275.

Supplemental Figures

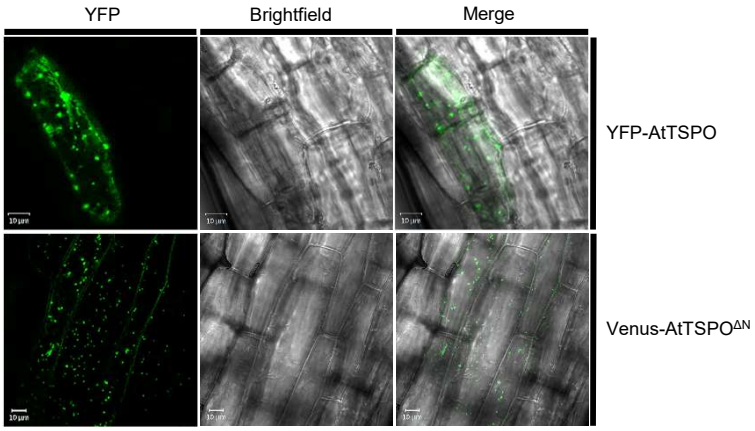

Figure S1. Subcellular localization of AtTSPO and AtTSPO$^{\Delta N}$ expressed in *Arabidopsis thaliana*. Related to Figure 5. Representative confocal images of hypocotyls of transgenic Arabidopsis seedlings overexpressing YFP-AtTSPO or Venus-AtTSPO$^{\Delta N}$. Full-length AtTSPO is detected in the Golgi membranes and in the ER and the N-terminus truncated AtTSPO localizes essentially to the Golgi. Bars = 10 µm.

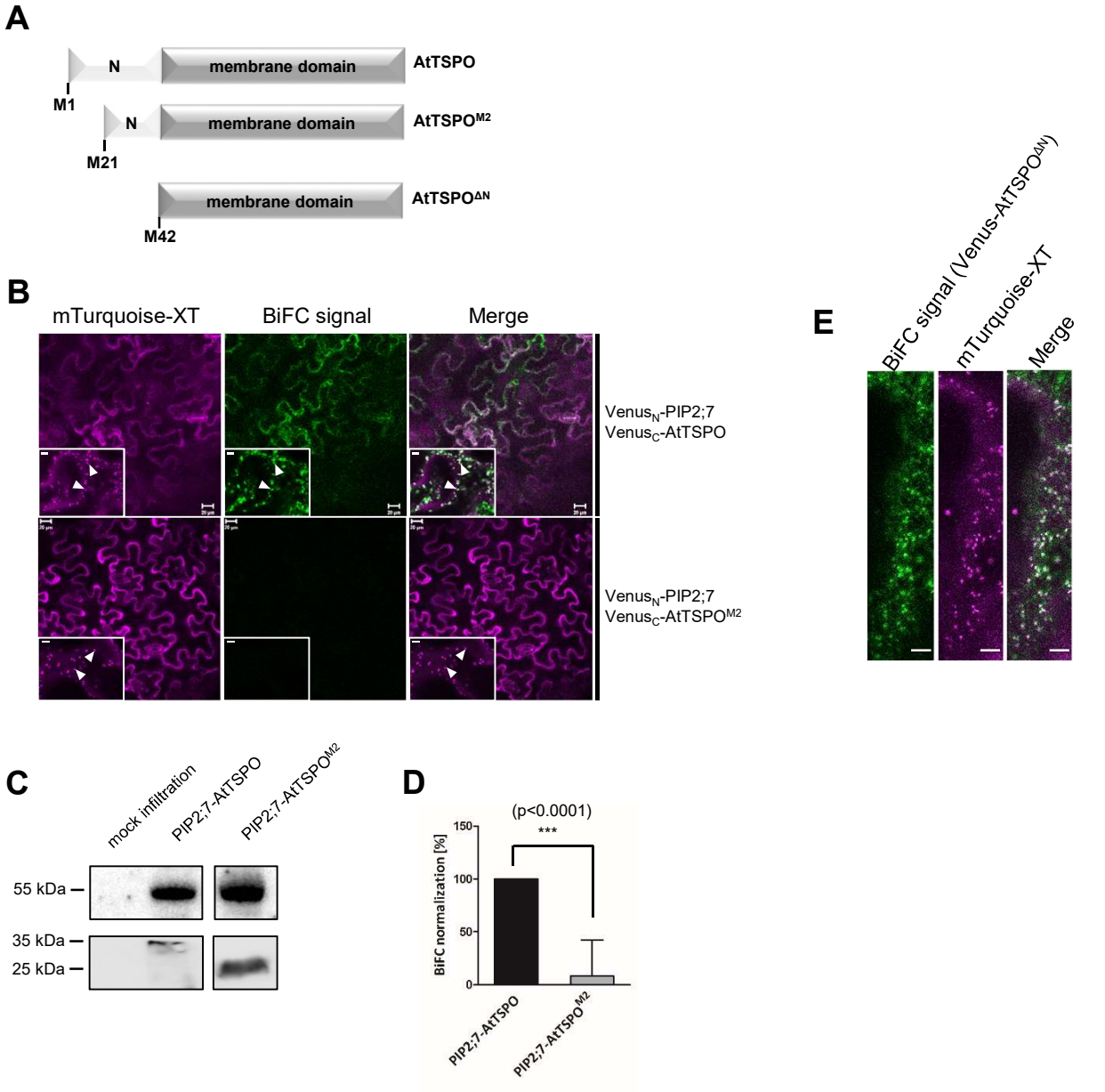

Figure S2. The first 20 amino acids of AtTSPO are also required for AtTSPO interaction *in vivo* with PIP2;7. Related to Figure 2. (A) Schematic representation of AtTSPO genetic constructs used in BiFC approach. As a positive control in this assay we used both full-length PIP2;7 and AtTSPO. N-terminus truncated variant (M2) starts with the methionine at the position 21, and the variant AtTSPO$^{\Delta N}$ starts with the methionine at the position 42. (B) BiFC assay on Agrobacterium-infiltrated *Nicotiana benthamiana* leaves. Xylosyltransferase-mTurquoise fluorescent chimera was imaged as cell transfection control (in magenta). Low magnification images qualitatively demonstrate occurrence or lack of BiFC (in green) and the insets with high magnification images show Golgi stacks (arrowheads). Bars = 20 µm and 5 µm for low and high magnification, respectively. Experiment was repeated at least twice. (C) Western blot of infiltrated leaves areas used for BiFC microscopy analysis (B). PIP2;7 expression was detected by anti-GFP. AtTSPO full-length and truncated form were detected by anti-FLAG (the tag was originally cloned in between Venus$_C$ and cloning site for AtTSPO). Non-infiltrated leaf area was used as a negative control. (D) Quantitative data of the signal show a drastic reduction of BIFC between PIP2;7 and truncated AtTSPO mutant as compared to full-length AtTSPO. For statistical significance evaluation an independent samples t-test was performed using Graphpad Prism 5 (San Diego, USA). Bars represent means +/- SD. See methods section for quantification procedure. (E) BiFC as in (B) but both AtTSPO and PIP2;7 cDNA were replaced by AtTSPO$^{\Delta N}$ coding sequence. The merge image shows colocalization between the BiFC signal (green) generated by interacting AtTSPO$^{\Delta N}$ and the fluorescence of the Golgi marker (magenta). Bars = 5 µm.

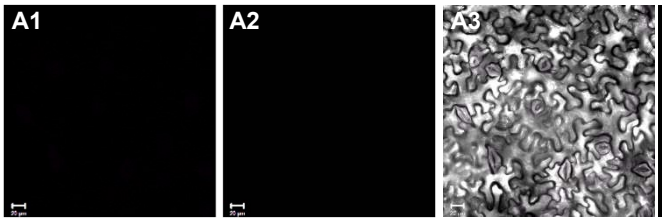

45.42 ± 13.57 | 15.00 ± 4.99 | ratio= BiFC/mTurquoise

Mock infiltration

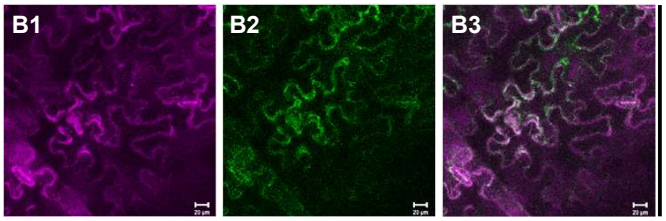

35.48 ± 30.45 | 9.11 ± 16.71 | ratio= 0.257 ± 0.660, norm.= 100%

$Venus_N$-PIP2;7
$Venus_C$-AtTSPO

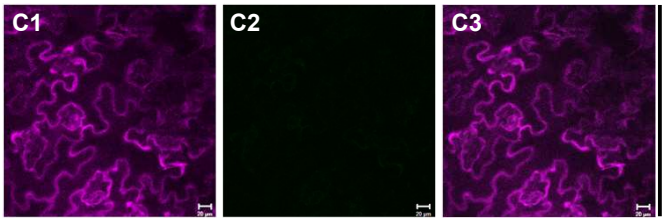

50.60 ± 43.48 | 1.48 ± 8.90 | ratio= 0.029 ± 0.198, norm.= 11.4%

$Venus_N$-PIP2;7
$Venus_C$-AtTSPO$^{\Delta N}$

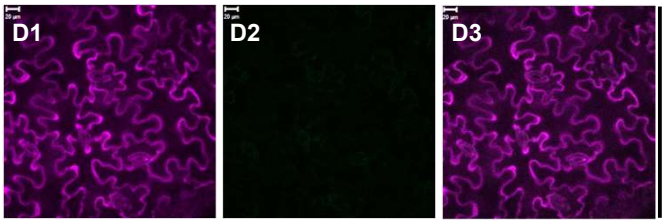

49.64 ± 42.56 | 1.04 ± 7.97 | ratio= 0.021 ± 0.176, norm.= 8.2%

$Venus_N$-PIP2;7
$Venus_C$-AtTSPO^{M2}

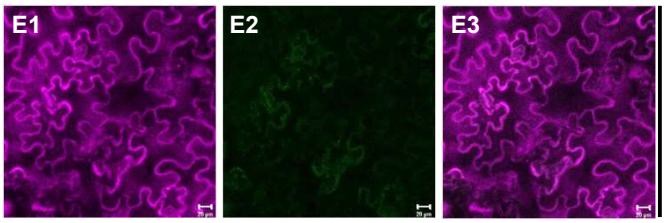

88.43 ± 59.65 | 2.91 ± 10.15 | ratio= 0.033 ± 0.130, norm.= 12.8%

$Venus_N$-PIP2;7
$Venus_C$-AtTSPO$^{K35A/R36A}$

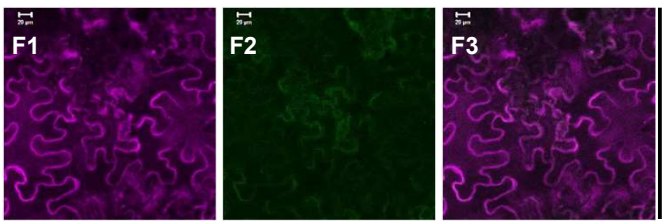

56.36 ± 45.92 | 2.78 ± 9.44 | ratio= 0.049 ± 0.200, norm.= 19.2%

$Venus_N$-PIP2;7
$Venus_C$-AtTSPO$^{K39A/R40A}$

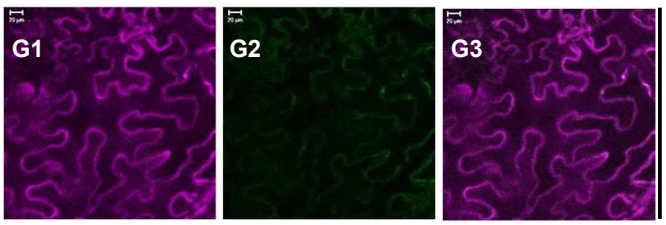

33.72 ± 33.96 | 1.53 ± 9.29 | ratio= 0.045 ± 0.321, norm.= 17.7%

$Venus_N$-PIP2;7
$Venus_C$-AtTSPO$^{K39A/R40A/K44A/R45A}$

Figure S3. Methodology of BiFC signal quantification. Related to Figure 2. Five independent randomly chosen (but not overlapping) areas of the infiltrated or non-infiltrated leaf were imaged. Pixel intensities from mTurquoise (magenta) and mVenus (green) channels were acquired along two diagonals of each image (around 700 intensity measurements per one diagonal) using ZEN2012 software (Zeiss). An average signal intensity was calculated from 10 diagonals (around 7000 intensities measurements). An average signal intensity from non-infiltrated leaves was subtracted. Ratio between an average BiFC/mTurquoise signal intensity was calculated and normalized against the control (combination PIP2;7-AtTSPO full-length).

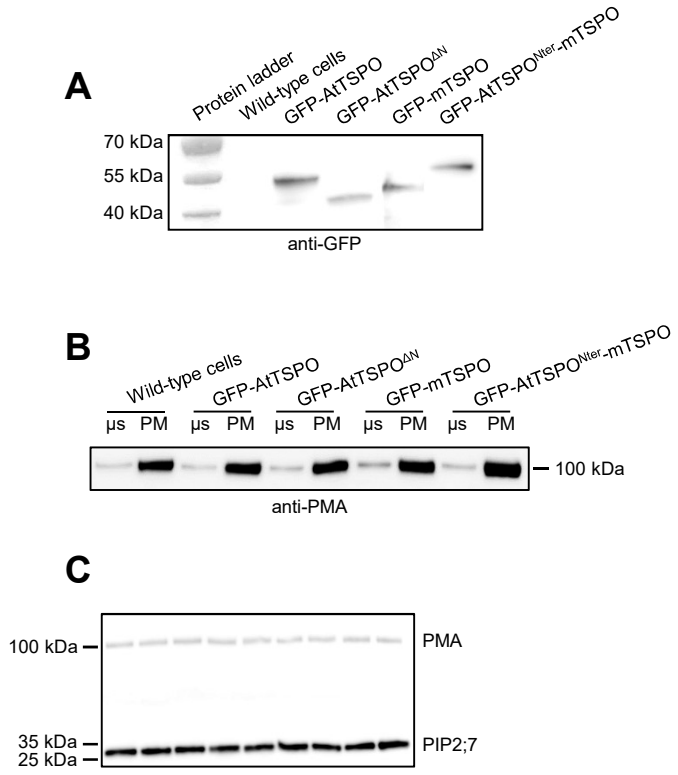

Figure S4. Representative Western blots for PIP2;7 aquaporin signal quantification in the plasma membrane-enriched fractions. Related to Figure 2. (A) Expression of GFP-TSPOs fusions in Arabidopsis PSB-D suspension cells. Each signal was exposed separately followed by superimposition on the protein ladder. (B) Preparation of plasma membrane-enriched fractions (PM) from Arabidopsis suspension cells. The plant plasma membrane H(+)-ATPase (PMA) was probed to check for relative enrichment (5 µg protein in each well); µs, microsomal fraction. (C) Relative amount of PIP2;7 aquaporin was checked by Western blotting. PMA was used as reference protein for the signal quantification. Shown is a representative membrane exposition. Both PMA and PIP2;7 were detected by specific antibodies.

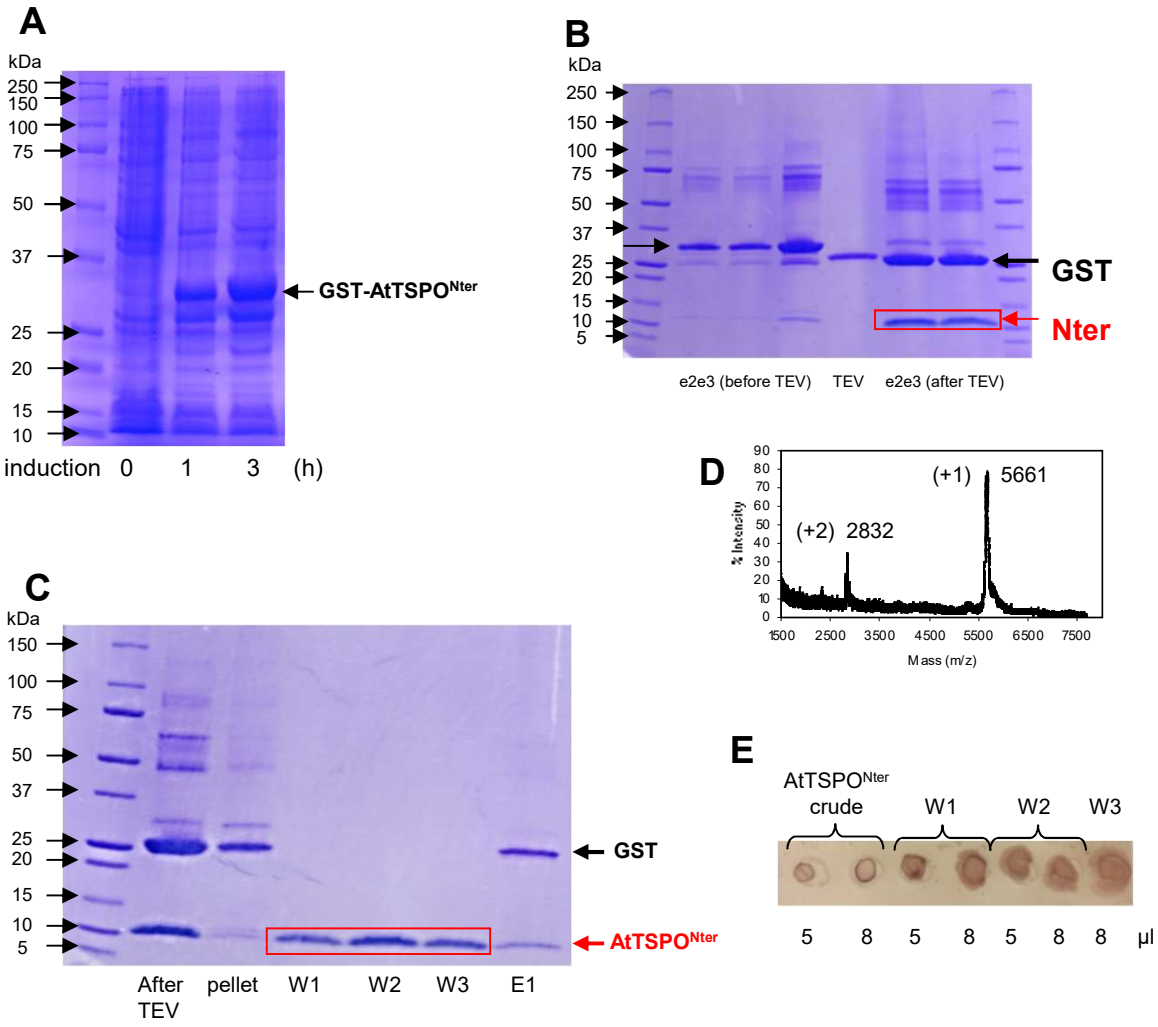

Figure S5. Expression, purification and characterization of the recombinant AtTSPO N-terminal peptide. **Related to Figure 3 and Figure 6.** (A) SDS-PAGE of bacterial culture samples taken along the expression time. (B) SDS-PAGE of elution fraction (e2 and e3) from the first step of bacterial cytosol purification containing fused protein GST-AtTSPO^{Nter} on Ni-NTA affinity column followed by dialysis to remove imidazole and further proteolytic digestion (TEV) to remove fusion protein (GST). (C) SDS-PAGE of the second step of purification on Ni-NTA column to remove His-tagged GST and His-tagged TEV proteins. Digested sample was centrifuged to remove GST precipitated as observed in the pellet. AtTSPO^{Nter} peptide was not retained on the column and collected by washing (W1-W3). GST was removed from the column by imidazole elution. (D) MALDI-TOF mass spectrum of purified AtTSPO Nter showing the expected molecular weight for [^{15}N] labelled peptide. (E) Dot blot of "crude AtTSPO^{Nter}" after proteolytic digestion, before final purification, and samples collected (W1-W3) after Ni-NTA purifcation.

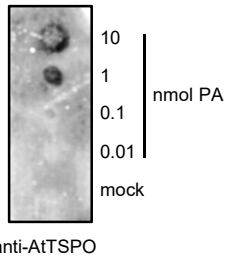

Figure S6. Purified AtTSPO N-terminal peptide binds phosphatidic acid (PA) *in vitro*. Related to Figure 3. Bacterially expressed and purified N-terminal peptide of AtTSPO was incubated with a spotted gradient of PA concentrations and detected with anti-AtTSPO antibodies. Experiment was repeated at least twice.

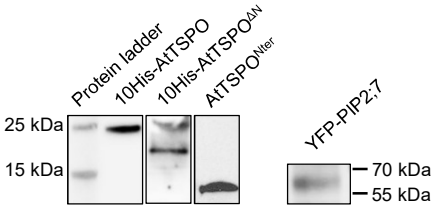

Figure S7. Representative western blot of protein samples used in thermophoresis experiments. Related to Figure 3, Figure 4 and Figure 6. AtTSPO and the truncated mutant were detected by HisProbe (Thermo Fisher Scientific) while the purified AtTSPO N-terminus peptide was detected using anti-AtTSPO antibodies. YFP-PIP2;7 fusion was detected using anti-GFP antibodies.

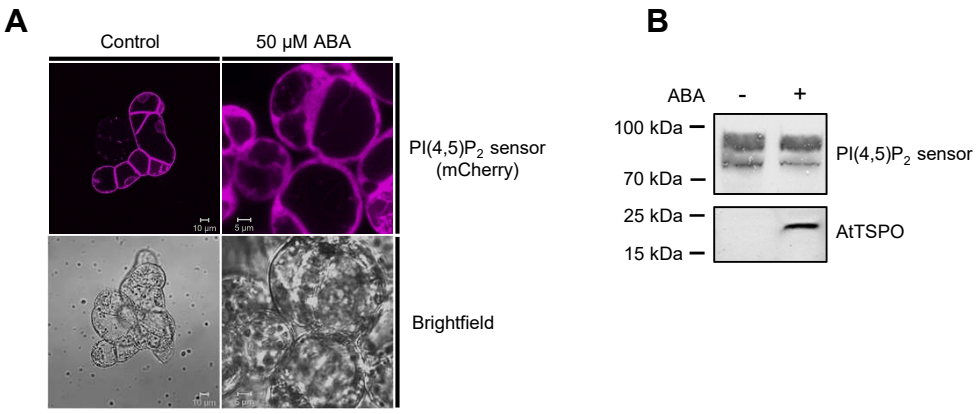

Figure S8. The PI(4,5)P_2 biosensor was depleted from the plasma membrane upon ABA treatment. Related to Figure 5. (A) Arabidopsis PSB-D suspension cells stably expressing the mCherry-tagged PI(4,5)P_2 sensor (double pleckstrin homology domain from phospholipase C) were treated with 50 µM ABA for 24h for endogenous AtTSPO induction. Control cells showed mCherry fluorescence mainly outlining the cell, most likely in the plasma membrane, and some intracellular signals in punctate structures around the nucleus. After ABA treatment, the mCherry fluorescence was essentially detected in the cytosol. Bars = 10 µm and 5 µm for control and treated cells, respectively. (B) Western blotting of ABA-dependent AtTSPO induction in cells imaged in (A). The lipid sensor was detected using anti-mCherry (Abcam ab167453) and served as a loading control. AtTSPO was detected using anti-AtTSPO antibodies.

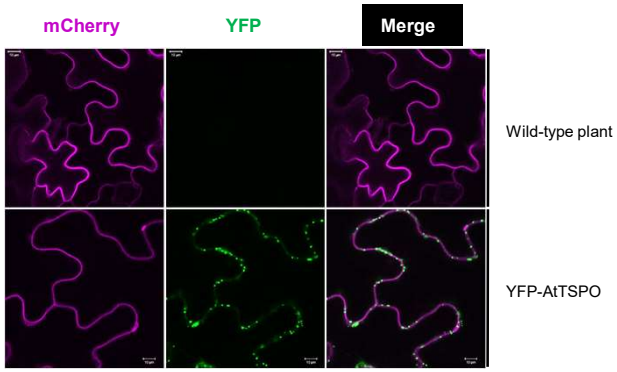

Figure S9. Expression of AtTSPO does not affect the targeting of PI4P 5-kinase to the plasma membrane. **Related to Figure 5.** The phosphatidylinositol 4-phosphate 5-kinase type-1 alpha fused to mcherry (mCherry-HsPIPK1a; in magenta) was transiently expressed in tobacco wild type or stably expressing YFP-AtTSPO (in green). Bars = 10 µm.

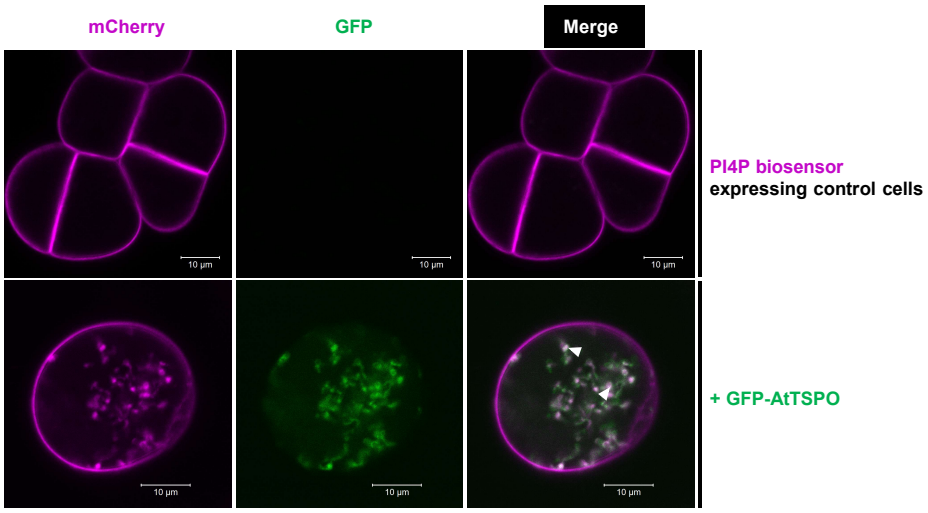

Figure S10. In presence of AtTSPO, the PI4P biosensor was partially depleted from the plasma membrane and partially colocalized with AtTSPO. Related to Figure 5. Representative confocal images of Arabidopsis suspension cells stably coexpressing the PI4P biosensor (mCherry-tagged double pleckstrin homology domain from Fapp1 protein; in magenta) and the full-length AtTSPO (GFP-tagged; in green). The arrowheads indicate mCherry and GFP signals colocalizing likely at Golgi membranes. Bars = 10 µm.

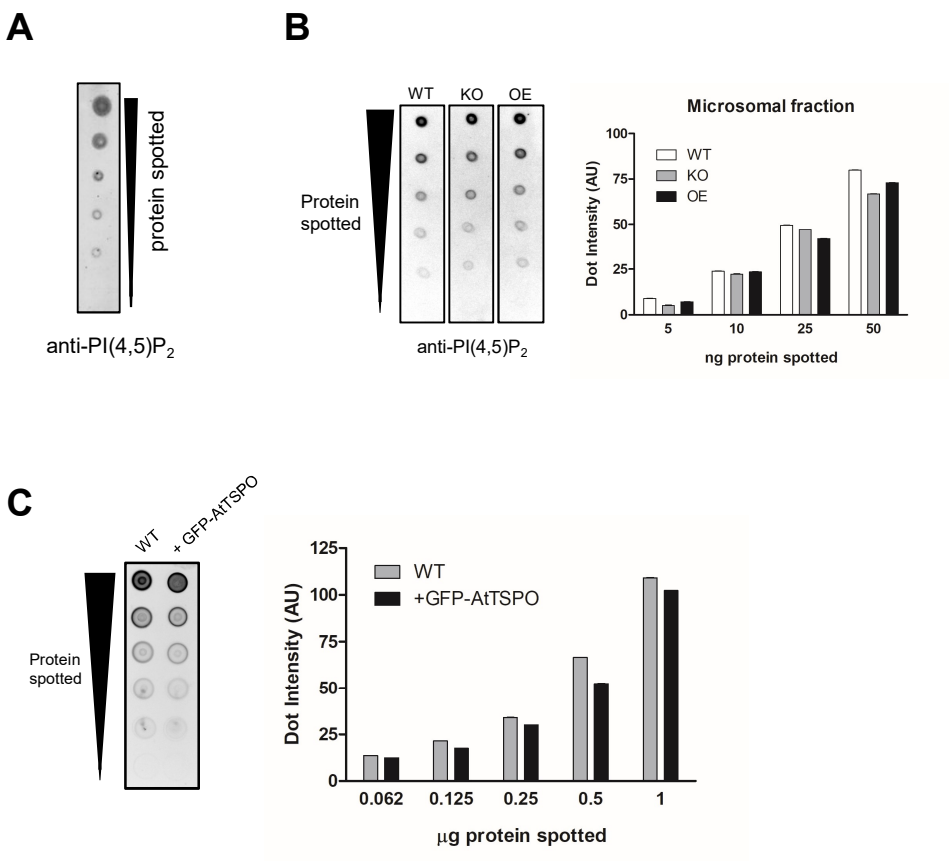

Figure S11. Overexpression of AtTSPO does not impact the overall content of PI(4,5)P_2 lipid in microsomal fraction. Related to Figure 5. (A) SDS-solubilized total extract of Arabidopsis plants was probed for PI(4,5)P_2 to validate the assay and antibodies. (B) SDS-solubilized microsomal fractions from the Arabidopsis wild-type (WT), knock-out for AtTSPO (KO) or AtTSPO overexpressing (OE) plant were spotted on the nitrocellulose membrane and probed for PI(4,5)P_2. (C) SDS-solubilized microsomal fractions from the Arabidopsis wild-type (WT) and GFP-AtTSPO overexpressing suspension cell lines were spotted on the nitrocellulose membrane and probed for PI(4,5)P_2. Average dot intensities were quantified using the ImageJ software and the plots represent a mean of three technical repetitions.

Supplemental Table S1. Primers used in this study. Related to figures 1-7.

Primers used to generate genetic constructs for BiFC analyses

Primer name	Sequence
SpeI-PIP2;7 Fw	5-AAAAAAAACTAGTATGTCGAAAGAAGTGAGCGAAGAAG-3
PIP2;7-XbaI Rv	5-AAAAAAATCTAGATTAATTGGTTGCGTTGCTTCGGAAC-3
AatII-AtTSPO Fw	5-AAAAAGACGTCCATGGATTCTCAGGACATCAG-3
AatII-AtTSPO^{M2} Fw	5-AAAAAGACGTCCATGGCCGAGACAGAGAGGAAAAG-3
AatII-AtTSPO$^{\Delta N}$ Fw	5-AAAAAGACGTCCATGGCGAAACGTGGTCTCAAG-3
AtTSPO-AsiSI Rv	5-AAAAAGCGATCGCTCACGCGACTGCAAGCTTTAC-3
AtTSPO^{K35AR36A} Int Fw	5-GACGACAACAAAGGAGCTGCTGATCAAAAGAGGGCGATG-3
AtTSPO^{K35AR36A} Int Rv	5-CATCGCCCTCTTTTGATCAGCAGCTCCTTTGTTGTCGTC-3
AtTSPO^{K39AR40A} Int Fw	5-GGAAAACGCGATCAAGCTGCTGCGATGGCGAAACGTG-3
AtTSPO^{K39AR40A} Int Rv	5-CACGTTTCGCCATCGCAGCAGCTTGATCGCGTTTTCC-3
AtTSPO$^{K39A/R40A/K44A/R45A}$ Int Fw	5-GAAAACGCGATCAAGCTGCTGCGATGGCGGCTGCTGGTCTCAAGTCTCTG-3
AtTSPO$^{K39A/R40A/K44A/R45A}$ Int Rv	5-CAGAGACTTGAGACCAGCAGCCGCCATCGCAGCAGCTTGATCGCGTTTTC-3

Primers used to generate genetic constructs expressed in Arabidopsis transgenic suspension cells

Primer name	Sequence
USER-kozak-GFP Fw	5-GGCTTAAUCCACCATGAGTAAAGGAGAAGAAC-3
GFP-AtTSPO Int Rv	5-CTGATGTCCTGAGAATCCATTTTGTATAGTTCATCCATG-3
GFP-AtTSPO Int Fw	5-CATGGATGAACTATACAAAATGGATTCTCAGGACATCAG-3
USER-AtTSPO Rv	5-GGTTTAAUTCACGCGACTGCAAGCTTTAC-3
L-GFP Rv	5- ACCAGCTCCAGCACCAGCTCCTTTGTATAGTTCATCCATG-3
L-AtTSPO$^{\Delta N}$ Fw	5-GGAGCTGGTGCTGGAGCTGGTCTGACGGTAGCGGTTGCG-3
GFP-mTSPO Int Rv	5-CACCCAGGATTCAGGCATTTTGTATAGTTCATCCATG-3
GFP-mTSPO Int Fw	5-CATGGATGAACTATACAAAATGCCTGAATCCTGGGTG-3
USER-mTSPO Rv	5-GGTTTAAUTCACTCTGGGAGCCGGGAG-3
USER-kozak-AtTSPO Fw	5-GGCTTAAUCCACCATGGATTCTCAGGACATC -3
AtTSPO^{Nter}-GFP Int Rv	5- GTTCTTCTCCTTTACTCATAGACTTGAGACCACGTTTC -3
AtTSPO^{Nter}-GFP Int Fw	5-GAAACGTGGTCTCAAGTCTATGAGTAAAGGAGAAGAAC-3

Primers used to generate TSPOs variants expressed and purified for biochemical analyses

Primer name	Sequence
XbaI-10His Fw	5-GGGGTCTAGAATGCATCACCATCACCATCACCATCACCATCAC-3
$10His^{C}$-AtTSPO Fw	5-CATCACCATCACCATCACATGGATTCTCAGGACATCAG-3
AtTSPO-XhoI Rv	5-AAAACTCGAGTCACGCGACTGCAAGC-3
XbaI-$10His^{N}$ Fw	5-GGGGTCTAGAATGCATCACCATCACCATC-3
10His-TEV^{N} Fw	5-CATCACCATCACCATCACCATCACCATCACGGTGAAAATTTATAC-3
TEV-$AtTSPO^{\Delta N}$ Fw	5-GGTGAAAATTTATACTTCCAAGGTATGGCGAAACGTGGTCTC-3
$AtTSPO^{\Delta N}$-XhoI Rv	5-GGGGCTCGAGTCACGCGACTGCAAGC-3
BamHI-10His-TEV^{N} Fw	5-GGGGGGATCCCATCACCATCACCATCACCATCACCATCACGAAAATTTATAC-3
TEV-$AtTSPO^{Nter}$ Fw	5-GAAAATTTATACTTCCAAGGTATGGATTCTCAGGACATCAGATAC-3
$AtTSPO^{Nter}$-XhoI Rv	5-GGGGCTCGAGTCAAGACTTGAGACCACGTTTC-3
NdeI-mTSPO Fw	5-AAAAACATATGCCTGAATCCTGGGTG-3
mTSPO-BamHI Rv	5-AAAAGGATCCTCACTCTGGGAGCCG-3
$AtTSPO^{Nter}$-mTSPO Int Fw	5-GAAACGTGGTCTCAAGTCTATGCCTGAATCCTGGGTG-3
$AtTSPO^{Nter}$-mTSPO Int Rv	5-CACCCAGGATTCAGGCATAGACTTGAGACCACGTTTC-3